RESEARCH ARTICLE

VOLCANICA

Precursory velocity changes prior to the 2019 paroxysms at Stromboli volcano, Italy, from coda wave interferometry

Alexander S. Yates*[α,β,γ], Corentin Caudron[α,β,γ], Aurélien Mordret[α,δ], Philippe Lesage[α], Andrea Cannata[ε,ζ], Flavio Cannavo[ζ], Thomas Lecocq[η], Virginie Pinel[α], and Lucia Zaccarelli[θ]

[α] Univ. Grenoble Alpes, Univ. Savoie Mont Blanc, CNRS, IRD, Univ. Gustave Eiffel, ISTerre, 38000 Grenoble, France.
[β] Laboratoire G-Time, Department of Geosciences, Environment and Society, Université libre de Bruxelles, Belgium.
[γ] WEL Research Institute, Avenue Pasteur, 6, 1300 Wavre, Belgium.
[δ] Department of Geophysics and Sedimentary Basins, GEUS, Geological Survey of Denmark and Greenland, Copenhagen, Denmark.
[ε] Dipartimento di Scienze Biologiche, Geologiche e Ambientali, Università degli Studi di Catania, Corso Italia 57, 95129 Catania, Italy.
[ζ] Istituto Nazionale di Geofisica e Vulcanologia - Sezione di Catania, Osservatorio Etneo, Piazza Roma 2, 95125 Catania, Italy.
[η] Seismology and Gravimetry Department, Royal Observatory of Belgium, Uccle, Belgium.
[θ] Istituto Nazionale di Geofisica e Vulcanologia, Sezione di Bologna, Bologna, Italy.

Submitted: 2024-07-19 | Accepted: 2025-03-18 | Published: 2025-05-11

Editor: E. Nicholson | Typesetter: J. Farquharson

Abstract

Open-conduit basaltic volcanoes are susceptible to sudden transitions from mild activity to violent explosive eruptions with little to no warning. Such was the case at Stromboli in the summer of 2019, when two paroxysmal explosions occurred within approximately two months (July 3 and August 28). We apply coda wave interferometry to identify possible transitions in behavior in the build-up to these events, computing seismic velocity changes using five broadband seismic stations on the volcano between 2013–2022. This timeframe encompasses a range of volcanic activity including effusive activity, major explosions and paroxysms. Cross-correlation functions are computed both between pairs of stations and single-station cross-components in multiple frequency bands that allow the sampling of different depths (between approximately 100–1000 m) within the plumbing system. Shallow velocity changes (1–2 Hz and 2–4 Hz) reveal mid-to-long term precursors prior to the paroxysms in 2019. For example, we observe that 2–4 Hz velocities recorded at the station closest to the active crater show an increase of 0.2–0.3 % relative to velocities recorded at other stations. This increase is largely accumulated from mid-2017, coinciding with previously observed heightened activity at the volcano, peaking approximately one month prior to the first paroxysm. A long-term decrease is also observed in deeper velocity changes (0.5–1.0 Hz) during the same time interval. It is hypothesized that these changes represent greater magma overpressure from increased volatile input from depth. The different response in the shallow subsurface may reflect a local response due to the same source within the vicinity close of the crater terrace. These findings illustrate how coda wave interferometry can provide meaningful insights into the evolving dynamics of open-conduit basaltic volcanoes.

Keywords: Coda wave interferometry; Volcano monitoring; Seismic velocity changes.

1 Introduction

Open-vent basaltic volcanoes are characterized by persistent explosive activity and passive degassing [Rose et al. 2013; Edmonds et al. 2022]. Such is the case at Stromboli volcano, Italy, where regular activity consists of 5–20 mild, discrete, explosions per hour [Harris and Ripepe 2007; Ripepe et al. 2013]. Occasionally, however, mild activity is interrupted by more significant events such as effusive eruptions, major explosions, and large violent explosions referred to as paroxysms [Métrich et al. 2005; Allard 2010; Rosi et al. 2013; Rizzo et al. 2015; Voloschina et al. 2023]. Such transitions in activity can occur with little to no warning, and thus represent a considerable hazard to inhabitants and visitors [Rosi et al. 2013]. Thus, techniques that can provide an indication of evolving behavior at open-vent volcanoes, and the transition to periods of heightened activity, are highly sought.

Stromboli is a small volcanic island located in the Southern Tyrrhenian Sea, within the northernmost part of the Aeolian archipelago. Its formation, as with other Aeolian Islands, is related to the subduction of African plate below the Eurasian plate [Barberi et al. 1974]. Only part of the volcano is above sea level, with a maximum elevation of 924 m [Bosman et al. 2009]. The submerged part of the volcano reaches approximately 2300 m below sea level [Bosman et al. 2009]. Current activity originates from three active craters (South-West, Central, and North-East) within the crater terrace (Figure 1) of the volcano [Salvatore et al. 2018].

Regular (mild) Strombolian activity at Stromboli is fed by crystal-rich, highly porphyritic (HP), basaltic magma residing at 2–4 km depth [Métrich et al. 2001; Landi et al. 2004; Métrich et al. 2009]. More explosive events, such as paroxysms and major explosions, release crystal-poor, low porphyritic (LP) basaltic magma originating from 7–10 km depth [Métrich et al. 2001; Francalanci et al. 2004; Métrich et al. 2009; Andronico et al. 2021]. High CO_2/SO_2 ratios during Strombolian explosions point towards a contribution of deep-derived gas from the LP storage zone during regular activity [Burton et al. 2007; Aiuppa et al. 2010; Aiuppa et al. 2021]. Thus it is considered that CO_2-rich gas bubbles are persistently supplied to the shallow plumbing system, which mix upon ascent with gases derived from the HP reservoir to drive Strombolian activity [Aiuppa et al. 2010]. For paroxysms, the trigger mechanism remains poorly understood, and various models have been considered [Aiuppa et al. 2021; Voloschina et al. 2023].

* alexander.yates@ulb.be

Two commonly considered models attribute pressure build-up to (1) the intrusion of new volatile-rich magma into the deeper system [e.g. Métrich et al. 2001; 2005] and/or (2) the accumulation of a foam layer at the top of the LP reservoir due to CO_2 degassing, followed by rapid rise of CO_2 rich gas to the surface [e.g. Allard 2010; Aiuppa et al. 2011; Aiuppa et al. 2021]. Note that these models are not necessarily mutually exclusive, rather it may be a question of which process is the dominant trigger force [Voloschina et al. 2023]. In any case, there is a general agreement that they result from the fast ascent and injection of deeply stored volatile fluids into the shallow plumbing system [Métrich et al. 2021].

More recent activity at the volcano has been marked by two powerful paroxysmal eruptions occurring on 3 July and 28 August 2019 [Giudicepietro et al. 2019; Inguaggiato et al. 2019; Giudicepietro et al. 2020; Inguaggiato et al. 2020; Calvari et al. 2021]. Both events produced eruptive columns more than 3 km high, followed by a pyroclastic flow that expanded along the Sciara del Fuoco slope [Giudicepietro et al. 2020; Inguaggiato et al. 2020]. The time between these events was characterized by intense volcanic activity consisting of frequent Strombolian explosions, spattering, lava overflows, and major explosions [Inguaggiato et al. 2020]. Combined, this period represents one of the most serious volcanic crises at Stromboli in the last decades [Giudicepietro et al. 2020]. Since then, short-term (minute-scale) ground tilt has been identified as a useful precursor for providing real-time warning of impending paroxysms [Di Lieto et al. 2020; Giudicepietro et al. 2020; Ripepe et al. 2021]. While short-term precursors can provide crucial warning time, identifying mid-to-long term precursors remains an important challenge for minimizing the impact of paroxysms.

Coda wave interferometry using the seismic ambient noise wavefield is an increasingly popular technique used for monitoring volcanoes [e.g. Sens-Schönfelder and Wegler 2006; Brenguier et al. 2008; Mordret et al. 2010; Donaldson et al. 2017; Yates et al. 2019; Calò et al. 2021; Caudron et al. 2022]. By cross-correlating continuously recorded seismic noise, it is possible to detect subtle changes in seismic velocity and structure of the medium through time. Such changes have been attributed to increased pressurization within the volcanic system [e.g. Brenguier et al. 2008; Mordret et al. 2010; Budi-Santoso and Lesage 2016; Yates et al. 2019; Calò et al. 2021; Caudron et al. 2021] and changes in fluid content [e.g. Caudron et al. 2015; 2022]. Furthermore, at Stromboli specifically, seismic velocity changes between 2011–2014 coincided with the timing of effusive activity [Calò et al. 2021]. These changes were resolved to regions matching previously known hydrothermal reservoirs, suggested to reflect pressurization in the hydrothermal system. Thus the technique is promising towards identifying mid-to-long term changes in volcanic systems (typically from weeks to years).

The sensitivity of seismic velocities to external, non-volcanic, processes often presents a challenge for monitoring volcanic processes. For example, rainfall has been identified to cause velocity changes at a number of volcanoes [e.g. Sens-Schönfelder and Wegler 2006; Rivet et al. 2015; Budi-Santoso and Lesage 2016]. Changes due to large tectonic earthquakes have also been observed to cause significant velocity decreases in volcanic settings [e.g. Brenguier et al. 2014; Yi et al. 2016; Machacca-Puma et al. 2019; Yates et al. 2019]. Outside of volcanic systems, changes related to temperature-induced thermoelasticity [e.g. Richter et al. 2014; Hillers et al. 2015a], atmospheric pressure loading [Silver et al. 2007; Niu et al. 2008], tidal modulation [Yamamura et al. 2003; Takano et al. 2014], and snow-loading [e.g. Hotovec-Ellis et al. 2014; Wang et al. 2017; Makus et al. 2023] have also been reported. While snow-loading is not relevant at Stromboli, the sheer number of identified processes causing velocity changes highlights the sensitivity of the subsurface to external forcing. Crucially, these changes are often of similar or larger magnitude than the volcanic processes of interest. Thus, one of the challenges is to carefully distinguish velocity changes related to volcanic processes from those related to external processes.

We compute seismic velocity changes between pairs of seismic stations and between different components of single-stations over a nine-year period from 2013 to 2022. This period encompasses a range of volcanic activity such as lava flows (including a flank eruption in 2014), major explosions, and three paroxysms. The third paroxysm, on 19 July 2020, was much smaller than the 2019 paroxysms, falling close to the threshold between a major explosion and a paroxysm [Calvari et al. 2021]. For station-pair cross-correlations, we use vertical component data recorded at different stations to target scattered seismic waves propagating between them in both directions. For single-station cross-correlations, we use the different components of a single station (east-north EN, east-vertical EZ, north-vertical NZ) to target energy that leaves a station before later returning as a scattered wave. The differences between both approaches lead to distinct spatial sensitivities according to the travel paths of recorded scattered arrivals, with single-station approaches shown to be highly sensitive to local changes [e.g. De Plaen et al. 2019; Caudron et al. 2022].

2 Methods

Data from five broadband seismic stations (Figure 1) that belong to the permanent network at Stromboli, run by Istituto Nazionale di Geofisica e Vulcanologia, were acquired during the period 2013–2022. These consist of three seismometers equipped with a Guralp CMG40T sensor (STRA, STR1, and STRE, 50 Hz sampling rate) and two with a Nanometrics Trilldedp ium 120 s sensor (ISTR and IST3, 100 Hz sampling rate). No instrument response correction is applied given all sensors have a flat response between frequencies of interest (0.5–4 Hz).

2.1 Computing cross-correlation functions and velocity changes

Using the `Python` software package `MSNoise` [Lecocq et al. 2014], cross-correlation functions are prepared using relatively established data processing methods that will be outlined briefly in this section. Complete parameter choices can be found in Supplementary Material 1 Tables S1 and S2. Seismic data for each day are grouped into continuous chunks, demeaned and merged into 1-day traces. Following this, traces

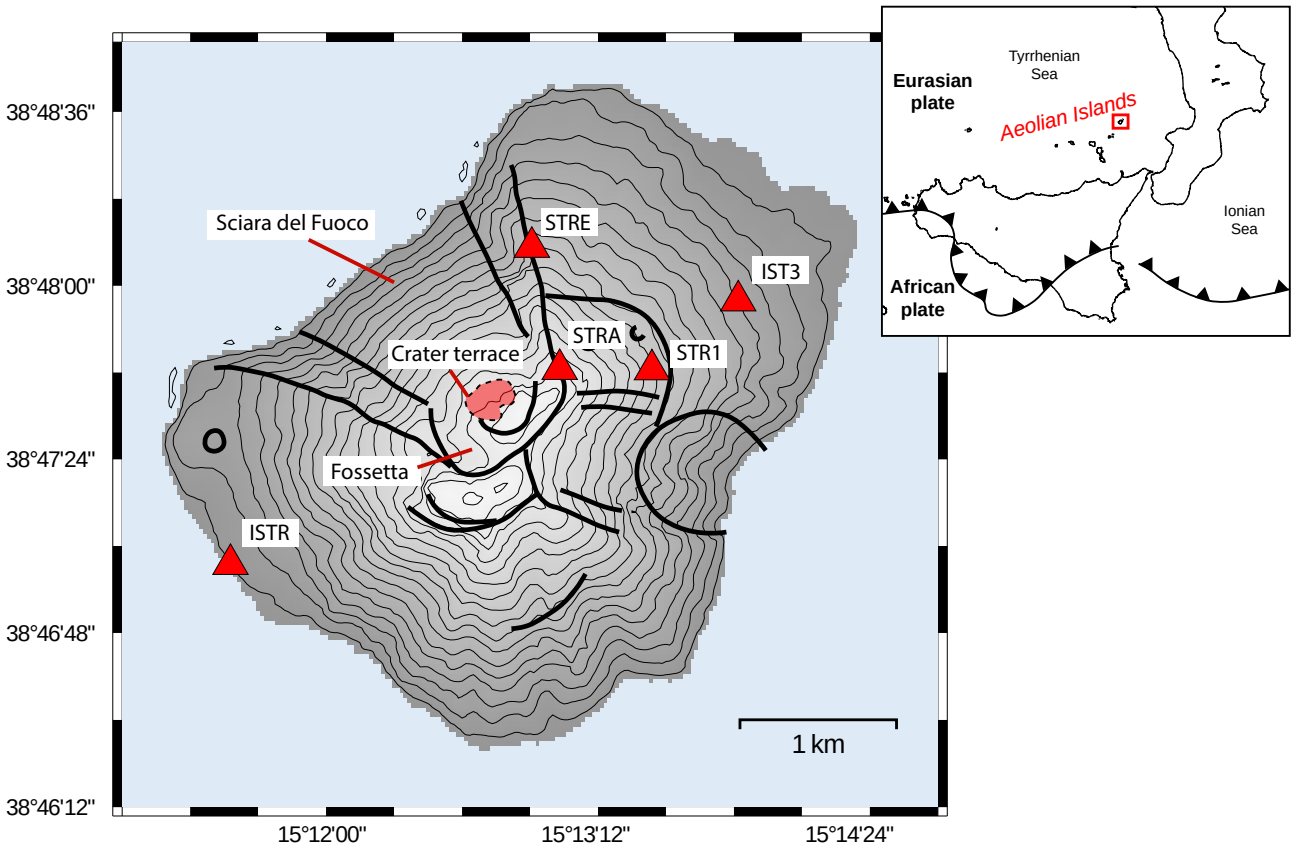

Figure 1: Map of Stromboli volcano, with broadband seismic stations used in this study shown as red triangles. Crater terrace, containing the three active craters, shaded red. Thicker black lines represent structural features (such as crater rims, lateral collapse rims, and caldera rims, [based on Revil et al. 2023, and references therein]. Inset (top right) shows location of Stromboli (red box) relative to broader regional setting.

are bandpassed between 0.01 and 10.0 Hz before being decimated to 25 Hz. For each individual station, and their three components, we then apply spectral whitening and 1-bit normalization in 30-minute windows. In order to study velocity changes at different frequencies, we apply whitening between 0.5–1.0 Hz, 1.0–2.0 Hz, and 2.0–4.0 Hz, providing three distinct data sets. The 30-minute windows are then used to compute the cross-correlation functions between various receivers. In this study, we compute vertical-vertical (ZZ) cross-correlation functions between pairs of stations and cross-component correlations (EN, EZ, NZ) between the components of a single-station. Finally, we perform linear stacking to give 5-day cross-correlation functions. Thus, the cross-correlation function recorded for a specific day represents the stack of that particular day and the preceding four days.

Velocity changes are computed using two commonly applied approaches: the stretching technique [e.g. Sens-Schönfelder and Wegler 2006] and the moving-window cross-spectral analysis technique [Poupinet et al. 1984; Clarke et al. 2011]. For the stretching technique, cross-correlation functions are stretched relative to a reference stack (stack of full time period here). We then seek the maximum value of the correlation coefficient between each current stack and reference stack at different levels of stretching up to factor of ±1 %. We do not observe any evidence to suggest velocity changes larger than this are present within our datasets. Once the maximum value is identified, the corresponding stretching coefficient is converted into an apparent velocity change and the correlation coefficient is recorded. For the moving-window cross-spectral analysis, delay-times between each cross-correlation function and a reference function are computed in a series of moving windows. The final velocity ($\delta v/v$) is calculated as the slope of delay times ($\delta t/t$) as $\delta t/t = -\delta v/v$.

For 0.5–1.0 Hz cross-correlation functions, the coda window is defined between 10–40 s lag time. For 1.0–2.0 Hz and 2.0–4.0 Hz, the coda is defined between 5–25 s and 5–15 s respectively unless otherwise stated. When applying the moving-window cross-spectral technique, we use sliding windows of 8 s, 4 s, and 2 s for 0.5–1.0 Hz, 1.0–2.0 Hz, and 2.0–4.0 Hz respectively, with a 50 % overlap. These lengths correspond to four cycles of the lowest frequency. Furthermore, we exclude delay time measurements if they are greater than 0.25 s, have an error greater than 0.1 s, or a coherence below 0.5. Similarly, for the stretching technique, results with a correlation coefficient less than 0.5 are excluded.

2.2 Complementary datasets

Daily precipitation, surface air temperature, and atmospheric pressure changes at sea-level are acquired as comparison datasets. Meteorological datasets for Stromboli itself were found to contain significant gaps that render them unsuitable for comparison with longer-term velocity changes. Thus, we rely on information that can be obtained from nearby stations. Precipitation data are obtained for Salina island, approximately 50 km from Stromboli. Temperature and atmospheric pressure data are obtained for stations at Messina and Catanzaro respectively from the Global Surface Summary of the Day (GSOD) dataset [National Climate Data Center 2013]. These stations show a strong similarity with values recorded at Stromboli during times this data are available (Supplementary Material 1 Figure S1).

For the daily precipitation data, we perform an additional step to estimate changes in pore pressure related to fluid diffusion, following Wang et al. [2017]. The one-dimensional complete diffusion equation established by Talwani et al. [2007] and later adopted by Rivet et al. [2015] underpins our computation of pore pressure variations ($P(r,t)$):

$$P(r,t) = \sum_{i=1}^{n} \delta p_i \operatorname{erfc}\left[r/(4c(n-i)\delta t)^{1/2}\right] \qquad (1)$$

In Equation 1, r refers to the distance (in this case, depth), n the total number of time increments δt between the start the time series (i=1) and time t. δp_i signifies the change in the precipitation load at the sampled instant t_i. This is calculated as $\rho g \delta h_i$, where ρ is the density (1000 kg m^{-3}), g the acceleration of gravity (9.81 m s^{-2}) and δh_i the variation in rainfall at the instance t_i from the previous day. The fluid diffusion rate, denoted by c, is measured in m^2 s^{-1}. For Stromboli, we compute the average pore pressure for r values ranging from 100 m to 1000 m (noting that deeper than this will be below sea-level). The optimal diffusion rate is estimated from the measured velocity changes, where we find the diffusivity that gives the maximum absolute value of the cross-correlation between velocity changes with the estimated pore pressures. This is discussed further in the Results section.

3 Results

Seismic velocity changes computed using the stretching-technique are presented for three different frequency bands in Figure 2, where we show the average for both single-station (averaging all stations) and station-pairs (averaging all pairs). Results applying the moving-window cross-spectral technique were found to be highly similar, shown in Supplementary Material 1 Figure S2.

In all frequency bands, we observe strong similarities between the results computed using pairs of stations and single-stations (Figure 2). Larger, approximately annual, periodicities are observed at higher frequencies, with variations on the order of ±0.5 % measured at 1.0–2.0 and 2.0–4.0 Hz during the nine-year period (Figure 2B and 2C). The annual nature of the data are confirmed when examining the spectral content of velocity changes, with a strong peak at approximately 365 days for 1.0–2.0 and 2.0–4.0 Hz (Supplementary Material 1 Figure S3B and S3C). At 0.5–1.0 Hz, velocities vary between ± 0.1 % (Figure 2A). The appearance of increased scatter in measurements at lower frequencies in Figure 2A can be related to the reduced amplitude of changes relative to the higher frequencies. Examining the spectra does reveal a peak at 365 days for single-station results (Supplementary Material 1 Figure S3A). Such a peak is less apparent in station-pair results.

Annual changes in seismic velocity are visualized more clearly by overlaying the velocity of each year in the different frequency bands (Figure 3). At higher frequencies (1–2 and 2–4 Hz), we observe a relatively consistent trend of low velocities in the early months of the year followed by high velocities in mid-to-late months (Figure 3B, 3C, 3E, 3F). At lower frequencies (0.5–1.0 Hz), we see a more subtle annual variation in single-station results, with higher velocities in the middle of the calendar year (Figure 3A). For station-pair results, minimal annual variation is observed (Figure 3D), consistent with the absence of a 365-day peak in the spectra (Supplementary Material 1 Figure S3A).

Of interest is the deviation of velocities from the annual trend in 2019. At 2.0–4.0 Hz, we observe that velocities increase in the months January to April during a time when velocities are usually at a minimum (Figure 3C, 3F). A similar observation is also present in the velocity changes for 1.0–2.0 Hz (Figure 3B, 3E). It is also interesting to note that velocities in 2019 (prior to the paroxysms) at both 1.0–2.0 and 2.0–4.0 Hz are higher than any other period during the nine years. At 0.5–1.0 Hz, velocities between May and July appear slightly lower than expected from usual trends (Figure 3A, 3D). Similarly, for the station-pair results, these velocities represent extreme values over the nine-year period, corresponding to the lowest recorded (Figure 4).

Comparing the annual velocity changes at higher frequencies (1–4 Hz) with the comparison datasets of temperature (Figure 3G), pore pressure changes (Figure 3H) and atmospheric pressure at sea level. (Figure 3I), we find that only pore pressures show a similar deviation from the average trend in 2019. For the pore pressures here, the diffusivity c is set to 0.02 m^2 s^{-1}, where this gave the maximum absolute value of the cross-correlation between modeled pore pressure changes and de-meaned velocity changes (2.0–4.0 Hz). Temperature and atmospheric pressure changes, on the other-hand, show minimal deviation from the average annual trend that can explain elevated velocity changes in the first few months of 2019. At lower frequencies (0.5–1.0 Hz), a drop in sea level pressure early 2019 coincides with a similar decrease in velocity. The velocity decrease between May and July, however, does not show a comparable change in sea level pressure. We do note though that the slight annual trend in the sea level pressure data is similar to that recorded at single-station, albeit inverse.

At lower frequencies (0.5–1.0 Hz), there is evidence of an evolving long-term trend over the nine year time period (Figure 4). This is revealed when applying smoothing to the original time series. From this an initially increasing velocity is observed between 2013–2015 before plateauing between 2015–2017 for both single-stations (Figure 4A) and station-pairs (Figure 4B). Velocities then begin to decrease from early 2017, reaching a minimum in early 2019 using station-pairs and

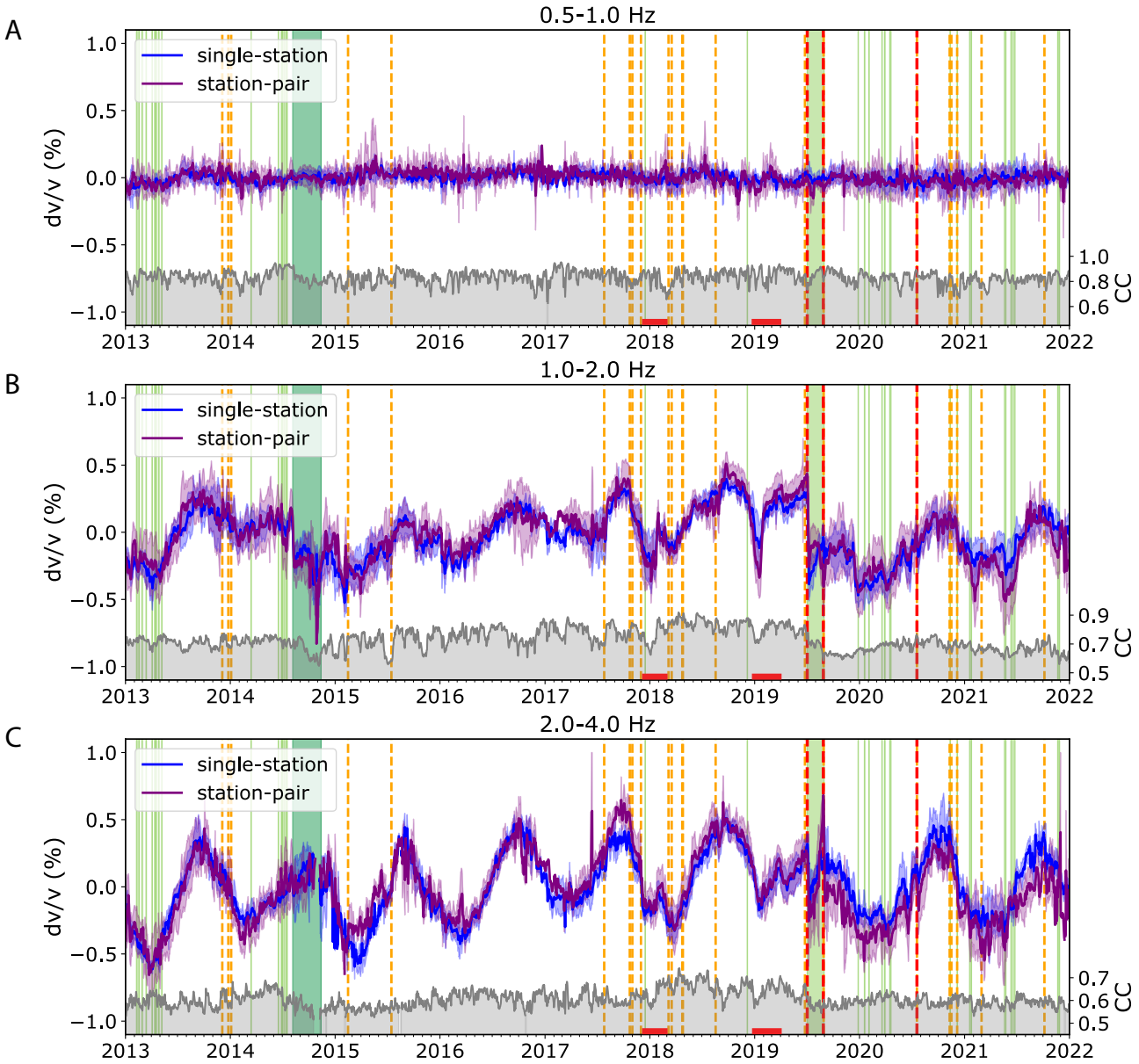

Figure 2: Velocity changes computed in three different frequency bands using stretching technique. Single-station velocities (blue-line) correspond to the average of all single-station cross-components (EN, EZ, NZ) for all stations. Station-pair velocities (purple) correspond to the average of all station-pairs (ZZ). Shading around velocity changes corresponds to one standard deviation of velocity changes—computed across different stations and/or components—before averaging. Correlation coefficient (CC) between 5-day moving stacks and reference shown as grey shading. Volcanic activity described by red-dashed-lines = paroxysms, orange-dashed-lines = major explosions, light-green-shading = lava flows, dark-green shading = 2014 flank eruption. Red bars above date-axis indicate timing of raised alert level in late 2017 and late 2018. [A] 0.5–1.0 Hz. [B] 1.0–2.0 Hz. [C] 2.0–4.0 Hz.

mid-2020 using single-station. From 2021, velocities appear to be increasing again using both pairs of stations and single stations. This time period is also associated with larger differences between individual velocity changes used in the averages, with some stations and station-pairs experiencing large changes during, or after, the 2019 paroxysms (Supplementary Material 1 Figure S4). Thus we observe larger standard deviations of velocity changes during this period (Figure 4).

At higher frequencies (2.0–4.0 Hz), examining the velocity changes recorded by individual stations reveals that STRA station (located closest to the summit) deviates from the other four stations in the months prior to the July 2019 paroxysm (Figure 5A). This is more clearly observed when comparing the velocity of STRA station with the average of the other four (Figure 5B), with the largest positive difference recorded one month before the July paroxysm (Figure 5C). It also ap-

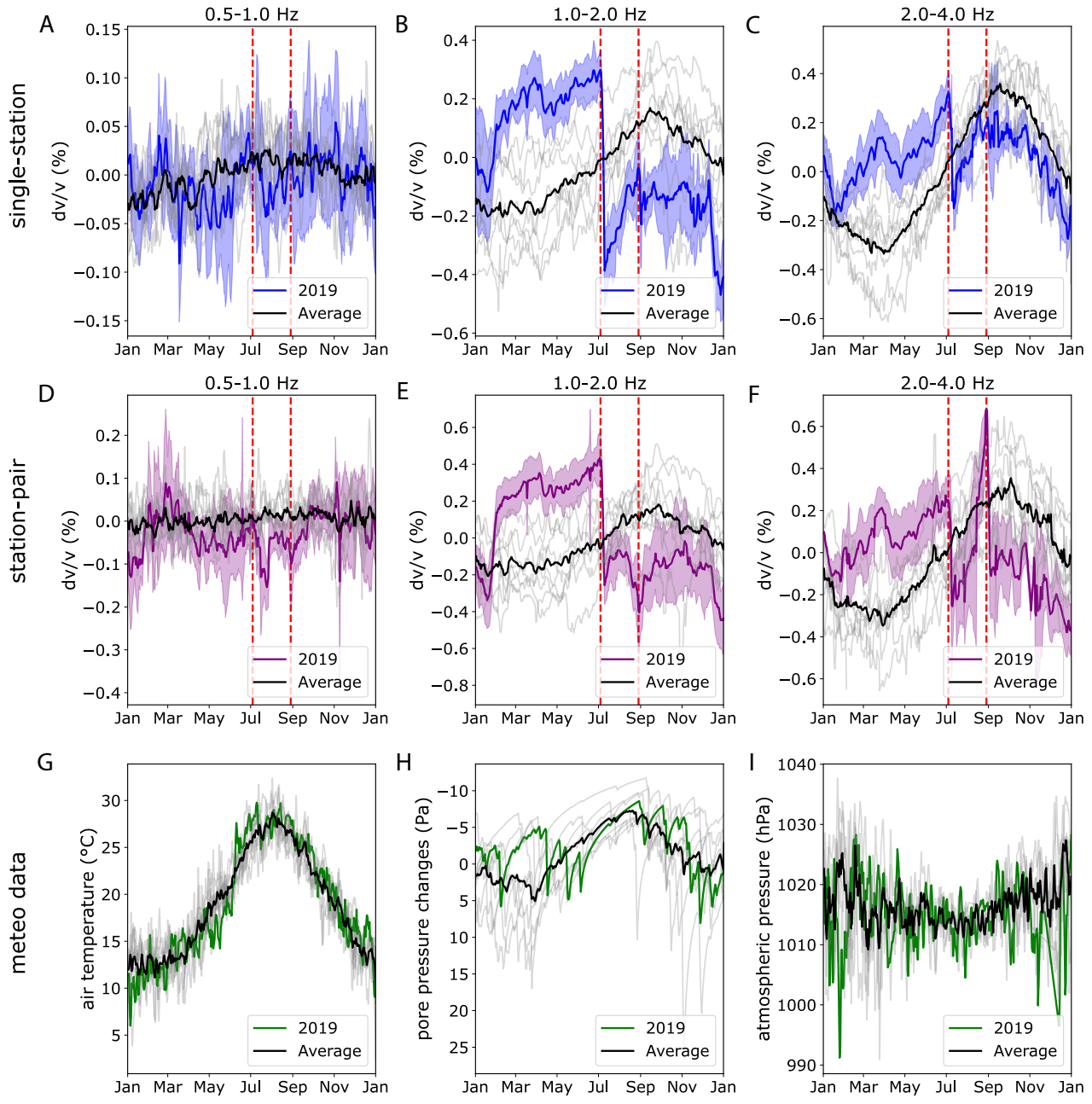

Figure 3: Single-station and station-pair seismic velocities (stretching technique) for each year plotted against calendar day, from 2013-01-01 to 2022-01-01, with various meteorological datasets also shown (including pore pressures computed from precipitation). Grey lines correspond to individual years with the exception of 2019 which is highlighted as different color (blue for single-station and purple for station-pair changes to match Figure 2), with one standard deviation shaded. For meteorological datasets, 2019 is colored in green and in all cases the average of all years (mean), excluding 2019, is shown as black line. The timing of the paroxysms in 2019 is indicated by red-dashed-lines. [A] single-station 0.5–1.0 Hz. [B] single-station 1.0–2.0 Hz. [C] single-station 2.0–4.0 Hz. [D] station-pair 0.5–1.0 Hz. [E] station-pair 1.0–2.0 Hz. [F] station-pair 2.0–4.0 Hz. [G] Temperature data. [H] Pore pressures, with c=0.02 m^2 s^{-1}. [I] Atmospheric pressure.

pears that the deviation of STRA station from the others may begin two years prior, with a positive difference mostly sustained from early 2017. Following the paroxysm, the velocity difference returns to approximately zero until the end of the dataset. A similar observation is also made prior to the 2014 flank eruption, with a positive velocity difference at STRA station sustained from mid-2013. The velocity difference subsequently decreases to values below zero just before the onset of the flank eruption.

These features are similarly resolved using the moving-window cross-spectral technique, albeit with more fluctuation in the daily relative difference (Supplementary Material

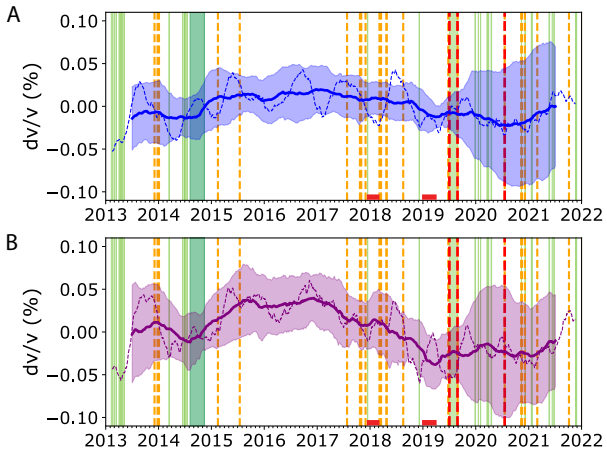

Figure 4: Smoothed 0.5–1.0 Hz velocity changes for both [A] single-station and [B] station-pairs (stretching technique). Dashed-lines represent 90-day smoothing window. Solid lines represent 365-day smoothing. Shading corresponds to one standard deviation of 365-day smoothed velocities used in average. Volcanic activity described by red-dashed-lines = paroxysms, orange-dashed-lines = major explosions, light-green-shading = lava flows, dark-green shading = 2014 flank eruption. Red bars above date-axis indicate timing of raised alert level in late 2017 and late 2018.

1 Figure S5). As with the stretching technique (Figure 5C), the relative difference at STRA station from early 2018 is consistently larger than (or approximately equal to) one standard deviation of all calculated differences (Supplementary Material 1 Figure S5C). An increasing trend in relative velocity difference is also resolved using 1–2 Hz cross-correlation functions between 2017 and the July 2019 (Supplementary Material 1 Figure S6). However, this is only sustained above one standard deviation from early 2019, and is not clearly elevated relative to other time periods (Figure 5C).

Finally, we observe sudden drops of velocity associated with the beginning of the 2014 flank eruption and the July 2019 paroxysms. This is best observed in the frequency band of 1.0–2.0 Hz (Figure 2B), where a velocity decrease of approximately 0.4 % is recorded in 2014 and 0.8 % in 2019. In both cases, the velocity does not seem to have recovered for a few years, with recovery still ongoing following the 2019 paroxysm by the start of 2022. At higher frequencies (2.0–4.0 Hz, Figure 2C), in contrast, minimal change is observed following the 2014 flank eruption and a 0.4 % velocity decrease is recorded following the July 2019 paroxysm. Drops in the correlation coefficient between 5-day cross-correlation functions and the reference are observed in both frequency bands.

4 Discussion

4.1 Deviating velocity at near-summit station

Two time periods are identified where the difference between 2–4 Hz seismic velocities recorded at STRA and the average of the four other stations are consistently above zero. These are: (1) from mid-2013 until just before the 2014 flank eruption, and (2) from early 2017 until the July 2019 paroxysm (Figure 5). From 2018 in particular, the relative difference is consistently above (or approximately equal to) one standard deviation of all calculated differences over the nine years. This peaks one month prior to the first paroxysm. During other time periods, including immediately following the onset of the 2014 flank eruption and the July 2019 paroxysm, the velocity difference stays closer to zero.

The position of STRA closer to the crater region should make it more sensitive to local changes around this part of the volcano. This can be demonstrated through the computation of 2D sensitivity kernels [e.g. Obermann et al. 2013; Planès et al. 2014; Budi-Santoso and Lesage 2016] using the analytical expression for the case of isotropic scattering of acoustic waves in the diffusion approximation, introduced by Pacheco and Snieder [2005] as:

$$K\left(s_1, s_2, x_0, t\right) = \frac{\int_0^t p\left(s_1, x_0, u\right) p\left(x_0, s_2, t-u\right) \mathrm{d}u}{p\left(s_1, s_2, t\right)}, \quad (2)$$

where s_1 and s_2 are the positions of the station, x_0 the position of a velocity perturbation, t the center of the lag time window used, and u the intermediate time interval over which the integration is performed. Thus $K\left(s_1, s_2, x_0, t\right)$ is the distribution of travel times of multiply scattered waves travelling from s_1 to s_2 after visiting x_0. For single-station kernels, we assign s_1 and s_2 as the same position [e.g. Caudron et al. 2022]. The function $p(s_1, s_2, t)$ represents the time-dependant t intensity at position s_2 due to a unit intensity impulse at s_1. For short times and when perturbations are close to the source or receiver, this can be described using the solution to the radiative transfer equation for the case of isotropic scattering media [Sato 1993; Paasschens 1997; Planès et al. 2014] following:

$$p(\boldsymbol{r}, t) = \frac{e^{-ct\ell}}{2\pi r}\delta(ct-r) + \frac{1}{2\pi\ell ct}\left(1-\frac{r^2}{c^2t^2}\right)^{-\frac{1}{2}} \exp\left[\ell^{-1}\left(\sqrt{c^2t^2-r^2}-ct\right)\right]\Theta(ct-r), \quad (3)$$

where r is the distance between s_1 and s_2, ℓ is the transport mean free path, c is the wave speed, δ the Dirac function, and Θ the Heaviside function. We set the transport mean free path ℓ to be 200 m, following estimates of Prudencio et al. [2015] at Stromboli, and 1 km s^{-1} for the wave speed c based on approximate maximum velocity of surface waves above 2 Hz estimated by Chouet et al. [1998]. Sensitivity kernels corresponding to a central lag time t = 10 s are shown for all station-pairs combined (Figure 6A), single-stations combined (Figure 6B), STRA station alone (Figure 6C), and the four stations IST3, ISTR, STR1, STRE (Figure 6D). When combining the kernels for multiple source/receiver pairs, the individual kernels are summed. The final presented kernels are then normalized by dividing by the maximum value.

From the kernels, we observe that the sensitivity for pairs of stations (Figure 6A) and the single-stations (Figure 6B) are highly similar, with far greater sensitivity to the North-Eastern portion of the edifice. This can explain the high similarity

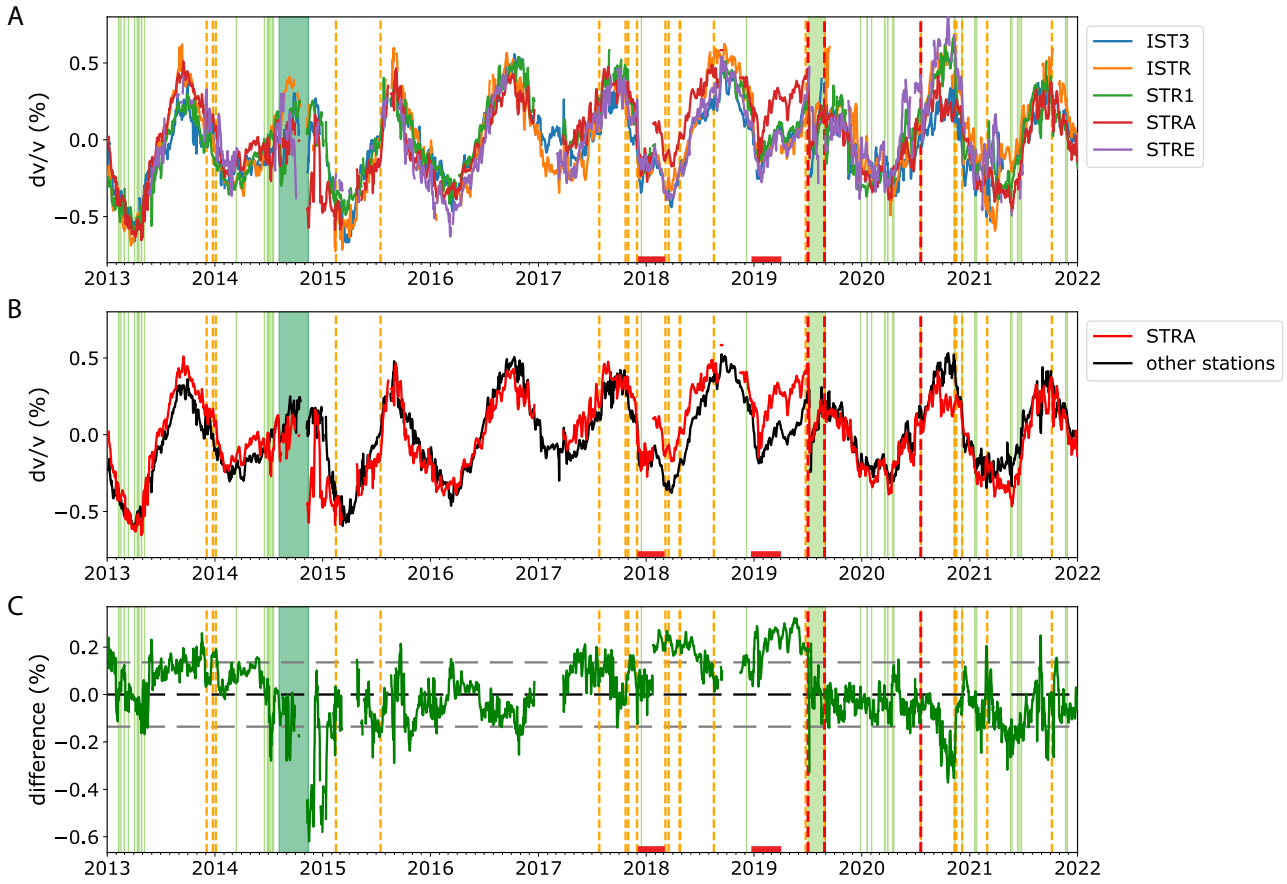

Figure 5: Comparing 2.0–4.0 Hz velocities (stretching technique) recorded at STRA station with other four stations. Volcanic activity described by red-dashed-lines = paroxysms, orange-dashed-lines = major explosions, light-green-shading = lava flows, dark-green shading = 2014 flank eruption. Red bars above date-axis indicate timing of raised alert level in late 2017 and late 2018. [A] Single-station seismic velocities for all stations. [B] Velocities for STRA station compared with average of IST3, ISTR, STR1, and STRE stations. [C] Difference between average velocity of STRA and other four stations. Grey dashed-lines represent one standard deviation of all calculated differences over the nine years either side of zero (black dashed-line).

between the station-pair and single-station results at Stromboli (Figure 2). There is a slightly greater sensitivity over the central and western portion of the edifice using station-pairs, however this is low relative to the north-eastern portion. Examining the kernel for STRA, we observe that there is a strong sensitivity to the crater region and the area just north-east of this (Figure 6C). In comparison, the combined sensitivity of the other four stations has very little sensitivity to the crater area (Figure 6D).

The observation of a larger velocity difference at STRA station in the 2–4 Hz frequency band—relative to 1–2 Hz—suggests differences in the shallow subsurface are important. The hypothesis is supported when examining the relationship of measured velocities with lag time (Supplementary Material 1 Figure S7). For example, the velocity changes measured at the four other stations show minimal variation when using later coda windows (Supplementary Material 1 Figure S7B). For STRA station, however, there is a clear decrease in the measured velocity between 2017 and the July 2019 paroxysm later into the coda (Supplementary Material 1 Figure S7A). Thus the difference in velocity between STRA and the other four stations also decreases at greater lag times (Supplementary Material 1 Figure S7C). Two possible explanations for this are considered. The first relates to the greater overlap in sensitivity kernels with increasing lag time. For example, using a central lag time of 20 s instead of 10 s shows that station STRA station becomes increasingly sensitive to velocities in the proximity of the other north-eastern stations (STR1, STRE, and IST3) (Supplementary Material 1 Figure S8C). Similarly, the average of the other four stations begin to show slightly greater sensitivity to velocity changes in the crater region (Supplementary Material 1 Figure S8D). Thus, it could be expected that the difference between stations will reduce with increasing lag time. Alternatively, it has been suggested that the contribution of body waves increases at later lag times [Obermann et al. 2013]. The effect of this is to increase depth sensitivity later into the coda. Thus, the decreasing velocities measured at STRA station with lag time between 2017 and July 2019 imply the shallow subsurface around STRA is responsible for the velocity difference between this station and

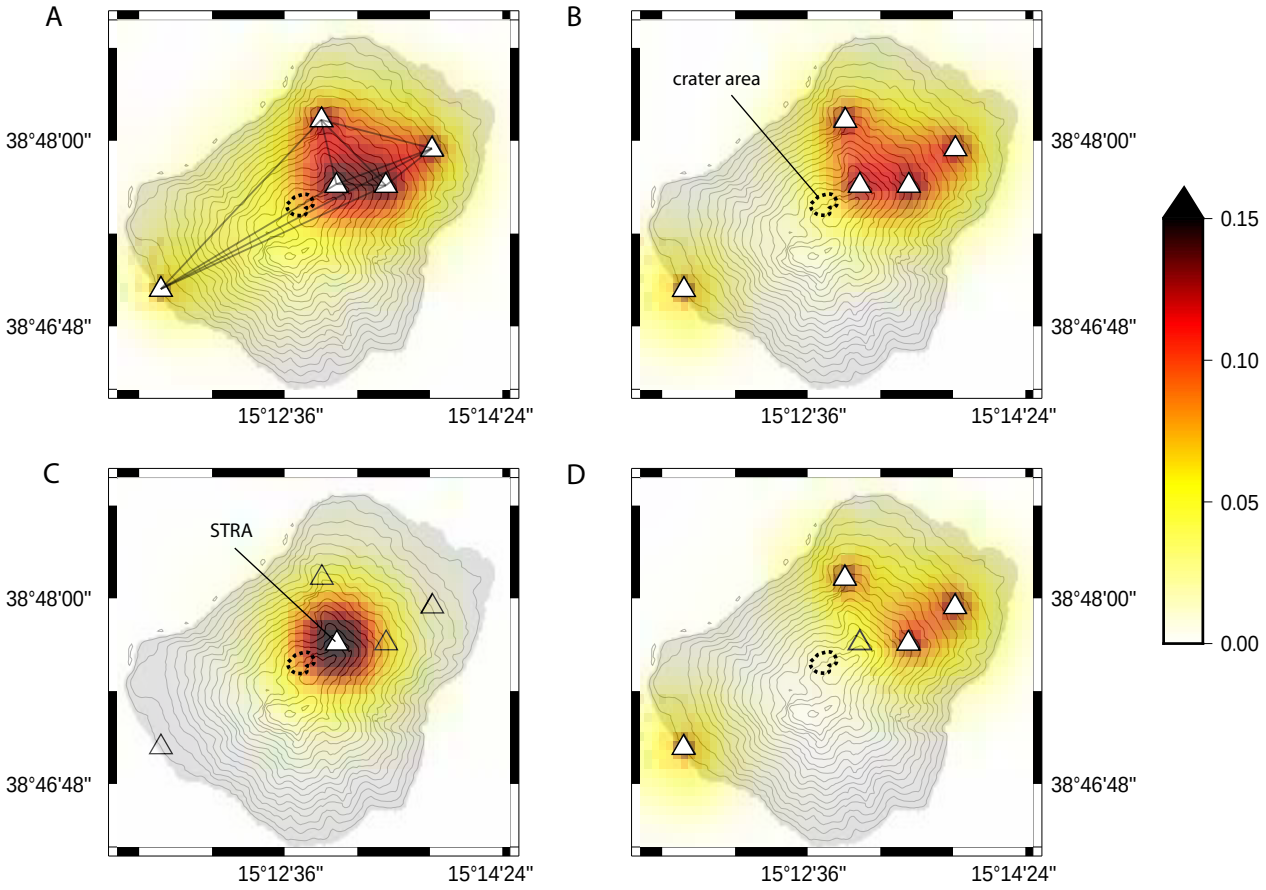

Figure 6: Lateral sensitivity kernels based on 10 s central lag time in the coda. All kernels are normalized with respect to the maximum value, and the color scale clipped at 0.15 for visualization (15 % of the maximum sensitivity). Higher values (darker colors) thus indicate areas more strongly contributing to measured seismic velocity changes. In each subplot, only contributing stations (triangles) are filled (white). [A] combined sensitivity of station-pairs, with transparent lines drawn that connect these pairs, [B] combined sensitivity of single-stations, [C] STRA station sensitivity only, [D] combined sensitivity of IST3, ISTR, STR1, STRE stations.

other stations. Note that the relationship between measured velocities and lag time is less clear for the period prior to the 2014 flank eruption at STRA (Supplementary Material 1 Figure S7A).

4.2 Environmentally-induced velocity changes

Annual velocity changes dominate higher frequency velocity changes at Stromboli, with measurements on the order of ±0.5% recorded between 1–4 Hz (Figure 2). The relation to a seasonal process is strongly suggested by the approximate 365-day periodicity of these changes (Supplementary Material 1 Figure S3). This is consistent with previous work of Calò et al. [2021], who identified seasonal changes at Stromboli at frequencies between 1.5–2.5 Hz between 2010 and 2013. At lower frequencies, evidence of seasonality is also identified when smoothing velocities to bring out the longer-term trend (Figure 4), noting that amplitudes are much smaller.

Seasonal changes in seismic velocity have been related to a number of meteorological processes. These include precipitation (groundwater changes) [e.g. Sens-Schönfelder and Wegler 2006; Rivet et al. 2015; Lecocq et al. 2017; Wang et al. 2017; Clements and Denolle 2018; Feng et al. 2021], temperature-induced thermoelastic strain [e.g. Meier et al. 2010; Richter et al. 2014; Hillers et al. 2015a; Lecocq et al. 2017], and variations in wind speed [Hillers et al. 2015a]. In the latter case, this is a non-physical change due to bias in velocity changes measurements caused by systematic noise excitation [Hillers et al. 2015a]. This is considered unlikely here, with the consistency between velocities computed using the stretching and moving window cross-spectral techniques (Supplementary Material 1 Figure S2) suggesting they reflect medium changes. This follows the assumption that, unlike the stretching method performed in the time-domain, the moving-window cross-spectral technique is less sensitive to variable frequency or amplitude of seismic sources [Zhan et al. 2013; Hillers et al. 2015b; Mao et al. 2020]. Atmospheric pressure changes have also been observed to influence seismic velocities on shorter-time scales [e.g. Silver et al. 2007; Niu et al. 2008]. However, the observation that daily fluctuations in atmospheric pressure are often larger than any seasonal trend suggests it is not the

dominant mechanism for higher frequency changes at Stromboli (Figure 3).

Precipitation and temperature-induced changes are both plausible mechanisms that may contribute to seasonal velocity changes at the volcano. Comparing these datasets with 2–4 Hz velocity changes—which recorded the largest seasonal variations—suggests a good fit with both datasets (Figure 7), with absolute correlation coefficients of 0.68 and 0.75 for precipitation (pore pressure changes) and temperature respectively. Note that this is negative for the comparison with pore pressure changes, indicating an inverse relationship. The corresponding delay time between velocity changes and these datasets is 44 days for temperature (Figure 7A) and 14 days for pore pressure changes (Figure 7B). For temperature-induced changes, such a delay between the source temperature field and resultant thermoelastic strain—approximately two to three months for annual changes [Ben-Zion and Leary 1986; Richter et al. 2014]—is anticipated. This relates to a number of factors, including the thermal diffusivity coefficient with depth and the presence of an unconsolidated surface layer [Ben-Zion and Leary 1986]. For precipitation-induced changes, some delay could be expected due to the time it takes water to percolate through the near-surface. For example, Andajani et al. [2020] observed delays of up to 1–3 weeks across many sites in south-west Japan, including through igneous rock. However, since a diffusion rate term is included in our estimation of pore pressure changes (in Equation 1), the observed delay more likely represents model misfit. This could relate to the contribution of other factors, such as aforementioned temperature-induced changes, but also to the limitations of the simple empirical model used here.

One argument potentially supporting an influence from rainfall may be the higher velocities recorded in 2019 relative to the average annual trend. At least for the first few months of 2019, the increase in seismic velocities (Figure 3B–3C and Figure 3E–3F) coincides with a decrease in pore pressures (Figure 3H). Yearly temperature measurements, in contrast, are far more consistent and thus provide no clear explanation to support any strong deviation in velocities from the annual trend. Thus our results might suggest both temperature-induced thermoelastic changes and precipitation-induced pore pressure changes contribute to measured seismic velocities. Determining the relative contribution of these two processes—at both 1–2 Hz and 2–4 Hz—is, however, outside the scope of this study.

At lower frequencies (0.5–1.0 Hz), a seasonal trend is clearly observed using single-station results (Figure 3A). The trend of these changes showed some similarity to the inverse trend of seasonal atmospheric pressures. A comparison of the two datasets (Supplementary Material 1 Figure S9) does not show a clear connection however, noting that atmospheric pressure changes are expected to be near instantaneous. Thus differences in phase between seasonal peaks suggest an alternative mechanism. Exploring this further is complicated without improved meteorological datasets (noting that these come from other more distant locations due to significant gaps at Stromboli).

Regarding the difference in sensitivity to seasonal processes using the single-station versus station-pair approach, this may relate to subtle differences in lateral sensitivity. Examining the velocities recorded by individual stations at low frequencies (0.5–1.0 Hz) shows a strong seasonal trend at IST3 station (Supplementary Material 1 Figure S10A). Comparatively, a seasonal trend is less evident at the other stations. This is confirmed when examining the spectra of velocity changes at individual stations (Supplementary Material 1 Figure S11. Previously computed lateral sensitivity kernel maps showed that the station-pair velocity changes had slightly greater sensitivity to the upper and western edifice of the volcano (Figure 6A) relative to the single-station velocity changes (Figure 6B). Thus, if the lack of a strong seasonal influence in low frequency velocity changes at STRA station is representative of the upper edifice response, it could be expected that a seasonal trend would be less clearly resolved by the station-pairs. Alternatively, it could be that there are slight differences in the depth sensitivity of the two approaches, considering only the vertical component was used for the station-pair approach. In contrast, the single-station approach uses the horizontal components which, unlike vertical components, have increased sensitivity to Love waves. This could result in the single-station sampling a shallower portion of the subsurface relative to the station-pairs. However, the lower amplitudes of velocity changes recorded at lower frequency, and thus difficulty distinguishing between medium changes and measurement error, make it challenging to draw strong conclusions.

Finally, we consider whether long-term trends in pore pressure changes can explain anomalous seismic velocities before the 2019 paroxysms. This includes both increasing and decreasing trends at high (Figure 3B–3C and Figure 3E–3F) and low (Figure 4) frequencies respectively, and the deviating velocity at STRA station (Figure 5). Examining the long-term trend of the modeled pore pressure changes (Figure 7C) reveals lower values from 2016 compared to previous years (2013–2015). However, much of this difference results from a large decrease in pore pressures from mid-2016 to early 2017 following a relatively dry year. Pore pressures then subsequently increase again through most of 2017, albeit still below pre-2016. In contrast, 2–4 Hz velocity changes record a long-term increase through both periods of pore pressure increase and decrease, peaking in early 2019 (Figure 7C). This is similarly true of the long-term decrease observed at lower frequencies (Figure 4). Thus, we consider that the long-term velocity anomalies observed prior to the 2019 paroxysms cannot be entirely explained by environmental factors.

4.3 Interpretation of velocity changes

The period from 2017 up until the 2019 paroxysms was marked by a re-awakening phase of the volcano, with various mid-to-long-term observations summarized in Figure 8A. From approximately May 2017, the volcano began to experience greater explosive activity, with increases in seismic signals such as volcanic tremor and Very Long Period (VLP) earthquakes (< 0.5 Hz [Giudicepietro et al. 2019]). The period also coincided with significant increases of CO_2 soil flux, following a long-term slowly increasing trend going back to

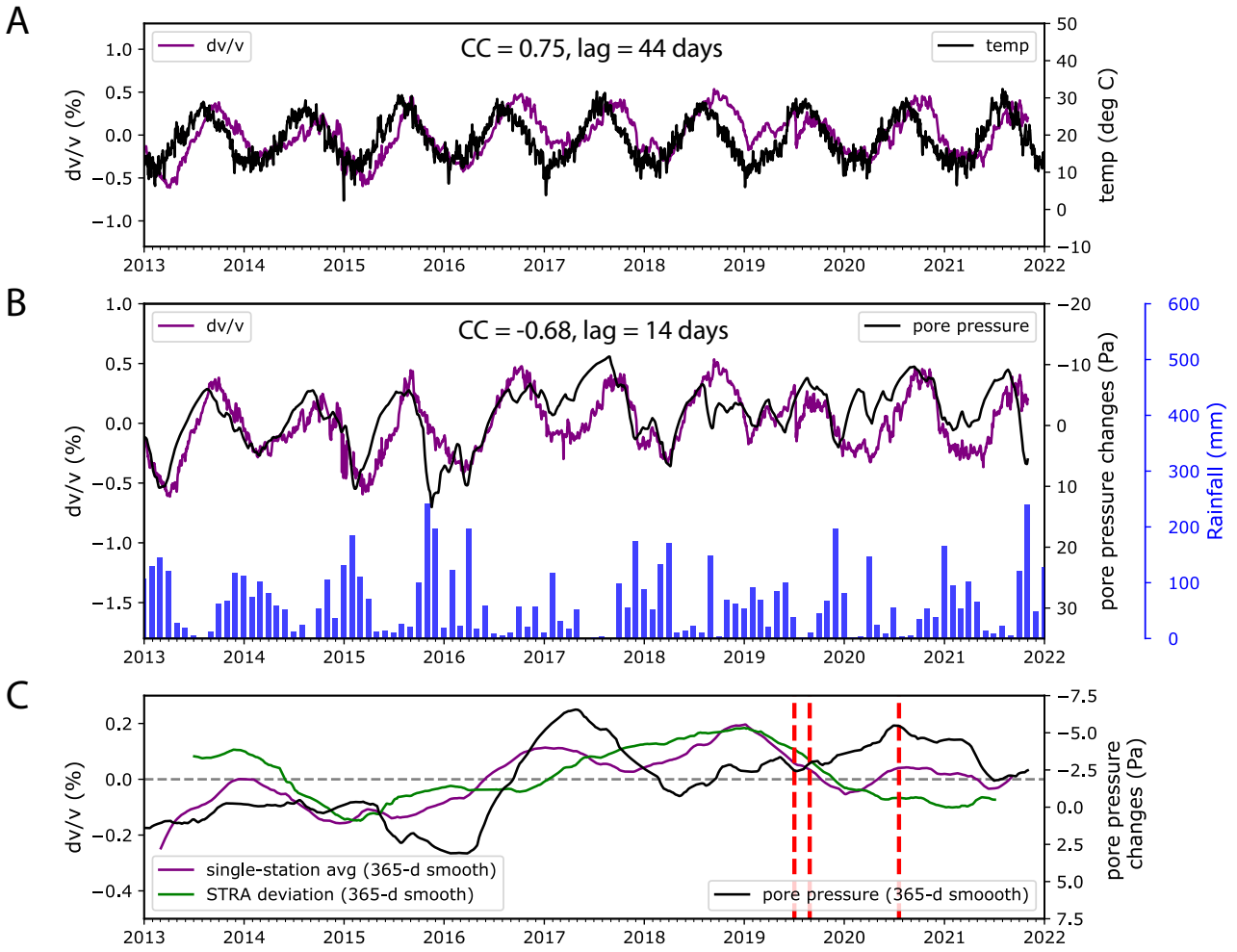

Figure 7: Single-station velocity changes at 2.0–4.0 Hz (avg. all stations, purple-line) compared with different meteorological data (black-lines). Correlation coefficient (CC) between datasets shown, computed at optimal lag/delay (also indicated). This reflects the time delay between [A] Velocities compared with temperature data. [B] Velocities compared with calculated pore pressure changes. Precipitation data used in pore pressure computations shown by blue bar-chart, binned by month. [C] Comparison between long-term (365-d smoothed) pore press changes and velocity changes, including the deviation of STRA station velocities as shown in Figure 5 (with a black dashed-line as zero %). Red-dashed-lines = paroxysms.

2005 [Inguaggiato et al. 2017; 2019; 2020]. In particular, the start of 2017 and late 2017/early 2018 (during the time period the volcanic alert level was raised from green to orange) were associated with significant increases in CO_2 soil flux [Giudicepietro et al. 2019; Inguaggiato et al. 2019; 2020]. A further trend of increasing soil gas flux was identified starting in late 2018, again associated with increases in volcano seismicity and, as a consequence, an increase in the volcanic alert level [Giudicepietro et al. 2019; 2020; Inguaggiato et al. 2020]. While the CO_2 flux was lower during this time period than the previous episodes in 2017 and early 2018, the rate of increase that continued up to the July 2019 paroxysm was greater than the overall trend in 2017–2018 [Inguaggiato et al. 2020]. Increased CO_2 plume degassing was also recorded from late 2019, peaking just before the paroxysm [Aiuppa et al. 2021]. Significant changes were similarly measured in VLP and tremor dynamics in the month prior to the onset of the July paroxysm [Giudicepietro et al. 2020]. These were interpreted to reflect higher gas content in the Strombolian explosive activity.

The observation of increasing CO_2 flux suggests a greater contribution from deeper stored magma, owing to its reduced solubility relative to other volcanic gases [Iwasaki et al. 1962; Aiuppa et al. 2010; Allard 2010]. Thus, periods of increasing CO_2 flux, coinciding with heightened explosive activity at the volcano, have been linked to the input of new CO_2-rich magmatic fluids into the deeper storage zone [Inguaggiato et al. 2019; 2020; Aiuppa et al. 2021; Inguaggiato et al. 2021]. This is also supported by an increased magmatic signature from low porphyritic (LP) magma in groundwater from mid-2017, increasing into 2018 [Federico et al. 2023]. The depth of this storage zone (7–10 km) is far deeper than the main depth sensitivity of measurements in this study (approximately <1 km, Supplementary Material 1 Figure S12). At the highest frequencies used (2–4 Hz), sensitivity is predominantly in the upper 200 m, with 1–2 Hz most sensitive within approximately

100–400 m, and 0.5–1.0 Hz within approximately 400–1000 m. Thus, our results are not directly sensitive to changes within the deeper LP storage zone. However, the relative increase in velocities at STRA station coinciding with increased explosive activity and CO_2 flux from 2017 up to the July 2019 paroxysm (Figure 5C) suggest we are sensitive to the response of the shallow system to volatile input from depth. These changes also coincide with a long-term velocity decrease during the same time period at lower frequencies (0.5–1.0 Hz, Figure 4). Thus we consider various mechanisms that can explain these observations in response to increased volatile input at depth.

Increased pressurization within the shallow plumbing system is one mechanism proposed to induce seismic velocity changes. Early studies at volcanoes identified velocity decreases in response to pressurization of the shallow plumbing system and inflation of the edifice [Brenguier et al. 2008; Duputel et al. 2009; Obermann et al. 2013; Rivet et al. 2014; Bennington et al. 2015; Cubuk-Sabuncu et al. 2021]. This is interpreted to result from an increase in the density of microcracks and thus causing a velocity decrease [Nur and Simmons 1969; Lockner et al. 1977; Brenguier et al. 2008]. However, some studies have identified velocity increases in response to pressurization. For example, velocity increases have been detected at Whakaari volcano (New Zealand) [Yates et al. 2019; Caudron et al. 2022], Ontake volcano (Japan) [Caudron et al. 2022], and Kīlauea (Hawai'i) [Donaldson et al. 2017; Hotovec-Ellis et al. 2022]. In this case, the interpretation is the closure of pre-existing microcracks under increasing pressure, thus causing a velocity increase [Nur 1971]. This difference reflects one of the challenges associated with interpreting seismic velocity changes at volcanoes, where both increases and decreases in velocity are possible. One explanation relates to the transition between elastic and plastic deformation with increasing strain. At small strains, velocities increase as microcracks close under increasing stress [Nur 1971], corresponding to the elastic regime. At larger strains, new cracks begin to develop and seismic velocities decrease [Nur and Simmons 1969; Lockner et al. 1977], indicative of plastic deformation. Thus, the observation of a velocity increase or decrease may relate to the relative position of the seismic stations to the pressure source. This was considered a possible mechanism at Merapi (Indonesia), where velocities decreased in the upper part of the edifice while velocities increased in the lower part of the edifice [Budi-Santoso and Lesage 2016]. Alternatively, the influence of the free surface, topography, and heterogeneity of volcanoes can induce both tensional and compressional stresses in different places [Got et al. 2013; Budi-Santoso and Lesage 2016]. Finally, it has been suggested that the mode of velocity change may be influenced by preferential crack orientation. This is suggested at Kīlauea, where a sensitivity to radial strain, rather than volumetric strain, is inferred as the cause of a velocity increase during pressurization rather than a decrease [Hotovec-Ellis et al. 2022; Muzellec et al. 2023].

An increase in magma overpressure at Stromboli, related to volumetric expansion due to the influx of CO_2-rich gas [Apuani and Corazzato 2009; Di Traglia et al. 2014; Inguaggiato et al. 2017], provides a plausible mechanism for inducing velocity changes. If this is accompanied by an increase in lava level within the conduit, an increase in the magmastatic pressure also acts on the conduit [Apuani and Corazzato 2009; Casagli et al. 2009; Di Traglia et al. 2014; Calvari et al. 2022]. This has been invoked to explain surface deformations within the summit area [Casagli et al. 2009; Di Traglia et al. 2013; 2014], with high CO_2 soil degassing also indicative of greater overpressure from new volatile-rich LP magma [Inguaggiato et al. 2011; Di Traglia et al. 2013; Inguaggiato et al. 2017; 2019]. Shorter-term fluctuations in deformation rates have also been related to variations in the magma flow rate within the plumbing system [Di Traglia et al. 2014]. During the period between April 2015 to June 2019, Synthetic Aperture Radar Interferometry (InSAR) measurements recorded small inflations of the crater terrace. This primarily occurred between December 2017 and January 2018 and December 2018 and January 2019 [Schaefer et al. 2019; Di Traglia et al. 2021]. Northward displacement of GPS station starting late 2016/early 2017—located towards the northern end of the island—also suggests modest inflation of the edifice occurred [Giudicepietro et al. 2019]. Similarly, inflation was recorded in the months prior to the 2014 flank eruption [Di Traglia et al. 2015; 2018]. Thus, there is evidence for increased magma overpressure acting on the conduit that could be responsible for observed velocity changes.

Long-term velocity changes measured at frequencies (0.5–1.0 Hz) are consistent with previous studies that identify a velocity decrease during pressurization of the shallow volcanic system [e.g. Brenguier et al. 2008; Rivet et al. 2014; Bennington et al. 2015; Calò et al. 2021]. In this scenario, the input of new, volatile-rich, magmatic fluid, creates an overpressure in the shallow system. For a spherical body, if the distribution of cracks in the surrounding rock is isotropic, a pressure increase induces tensile mean normal stresses [McTigue 1987], promoting a seismic velocity decrease. Thus, we suggest that the decreasing trend starting from early 2017 at low frequencies captures increased volatile input into the shallow volcanic system at Stromboli, consistent with other observables during the same time period [e.g. Giudicepietro et al. 2019; Inguaggiato et al. 2019].

For the increasing velocity recorded by the summit station at higher frequencies, it is important to consider the use of the relative velocity difference between seismic stations. A deviating velocity at STRA station doesn't necessarily imply the source is close to the crater area. For example, a velocity decrease present at all stations, with reduced influence closer to the summit area, would also record a relative increase at STRA station. Similarly, a broad velocity increase, with greater influence at the summit, would show the same effect. Thus it is necessary to consider both scenarios i.e. a localized velocity increase in the vicinity of the crater terrace (Figure 8B) or a broad velocity decrease (or increase) over the edifice with reduced (or greater) influence within the crater terrace area (e.g. Figure 8C).

Localized velocity increases have been previously identified close to active craters at both Whakaari and Ontake volcanoes [Yates et al. 2019; Caudron et al. 2021; 2022]. These were interpreted as due to gradual sealing of eruptive vents within the shallow hydrothermal system and subsequent pressure build-

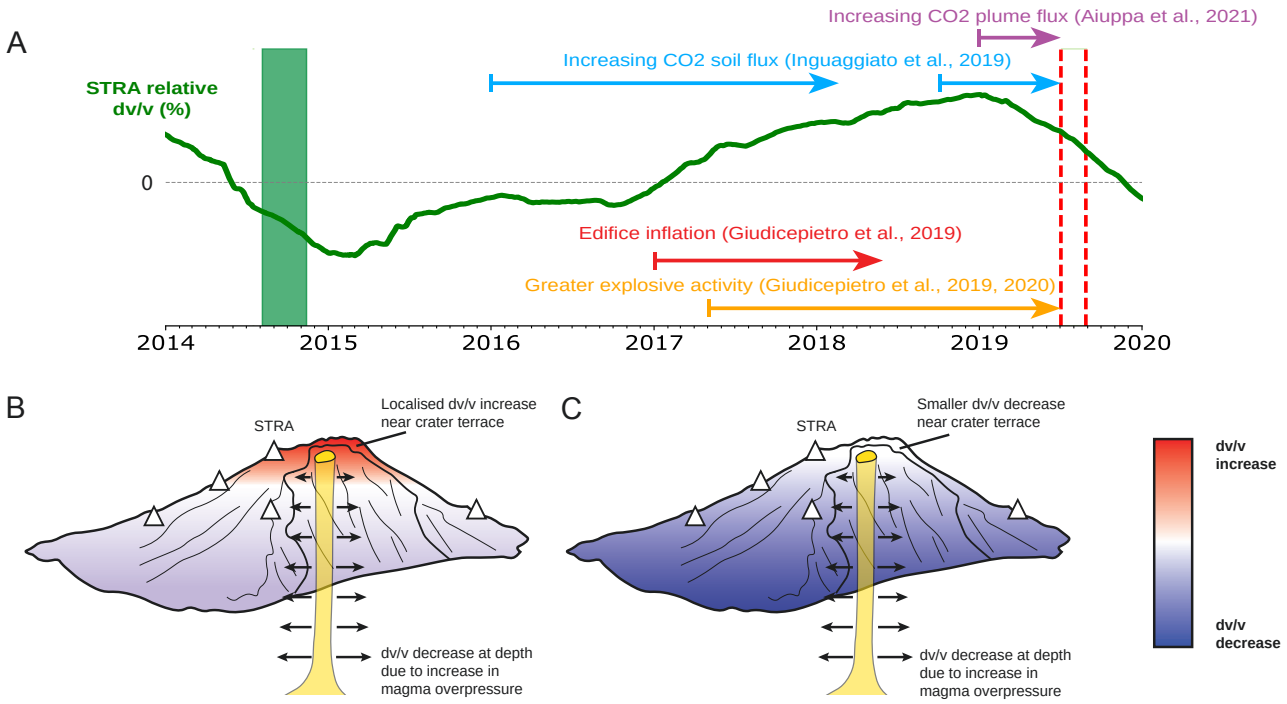

Figure 8: Various mid-to-long term observations at Stromboli and two conceptual models that may explain relative increase at STRA station in response to increased magma overpressure. [A] Observations at Stromboli prior to 2019 paroxysms compared with relative increase of velocity at STRA station (smoothed using 365-d moving window for visual simplicity). Red-dashed-lines = paroxysms, dark-green shading = 2014 flank eruption. [B] Model one: Local velocity increase near the crater terrace with velocity decrease at depth. [C] Model two: Broad velocity decrease, with reduced influence near the crater terrace.

up. At Stromboli, the existence of a seal within the hydrothermal system has been identified—just west of the active craters (in the Fossetta)—based on low levels of soil CO_2 in this area [Finizola et al. 2002; Revil et al. 2011]. However, there is no suggestion that significant buildup of pressure occurs beneath this seal, with structural boundaries only considered to impede and re-direct fluids [Revil et al. 2004; 2023]. Alternatively, it has been suggested that a crystal-rich, semi-permeable, plug exists in the upper several hundred meters of the conduit at Stromboli [Suckale et al. 2016; McKee et al. 2022]. This can act as a mechanism for gas accumulation, where gas can become trapped in pore spaced between crystals within the plug or at the base of the plug [Belien et al. 2010; Oppenheimer et al. 2015; Oppenheimer et al. 2020]. The build-up of overpressure due to gas accumulation and eventual overcoming of the plug yield strength is then thought to be the trigger for regular Strombolian explosions [Suckale et al. 2016; Oppenheimer et al. 2020; McKee et al. 2022]. However, it is not expected that significant overpressure can be sustained within the plug [Suckale et al. 2016]. Thus it is difficult to explain a long-term pressure build-up beneath a crystal plug within the upper conduit as the cause for the increasing relative velocity over approximately two years.

There is some suggestion that the timing of inflation events in the crater terrace area—coinciding with raised alert levels in late 2017/early 2018 and late 2018/early 2019—is related to the increasing relative velocity at STRA station. For example, it is during both of these periods that the relative difference rises above one standard deviation of all calculated differences (Figure 5C). However, it can also be argued that the start of these periods of heightened activity (marked by red bars in Figure 5) are associated with sharp, temporary, velocity decreases at all stations. This same result was found when computing velocity changes using highly similar cross-correlation functions produced during heightened activity [Yates 2023] and is also consistent with the results of Calò et al. [2021]. They identified short-term velocity decreases across the whole edifice associated with periods of heightened activity within a similar frequency band (1.5–2.5 Hz [Calò et al. 2021]). Thus an interpretation of increasing seismic velocities around the crater terrace due to increasing magma overpressure appears contrary to previous interpretations.

One possibility could be differences in how the crater terrace area responds to pressurization relative to the rest of the volcanic edifice. The magnitude of magmastatic pressure is expected to be minimal at the surface [Iverson 1995; Apuani and Corazzato 2009], instead increasing with depth. Thus, a velocity decrease due to increased in magma overpressure—as suggested at lower frequencies—could have a smaller influence near the summit (e.g. Figure 8C). Furthermore, previous numerical modeling of deformation based on magmastatic pressure supports that the response to stresses could be highly localized at Stromboli [Apuani and Corazzato 2009]. Alternatively, structural features may play a role in how the edifice re-

sponds to pressurization. The summit area of Stromboli contains many fractures (ring faults) associated with old collapse events [Finizola et al. 2009], shown in Figure 1. Measurements of dilation direction based on these features indicate a dilation direction perpendicular to these collapse scarps [Tibaldi et al. 2003]. If micro-cracks responsible for velocity changes are similarly orientated with these larger features, it may be that radial strain is a more important factor than tensile strain in the response to pressurization near the crater terrace [Hotovec-Ellis et al. 2022; Muzellec et al. 2023]. The velocity change at STRA station may then be different relative to parts of the edifice with a more isotropic crack orientation. This could be either a localised velocity increase due to dominant sensitivity to radial compressive stresses (e.g. Figure 8B), or simply a reduced sensitivity to tensile stresses (e.g. Figure 8C). Numerical modeling of the volcanic system would be necessary to further test these hypotheses, combined with a more complete understanding of microcrack orientations/anisotropy.

A final consideration is how a change in the ratio of gas might influence seismic velocity changes. Increased gas saturation is expected to decrease P-wave velocities, with limited influence on S-wave velocities [Nur and Simmons 1969; Lumley 2010; Clarke et al. 2020]. Since the coda are primarily sensitive to shear-wave velocity [Snieder 2006], it is not expected changes in the proportion of gas would have a significant influence. However, if pore water were to convert to steam—through the interaction of rising, high temperature, volatiles—an increase in pore pressures could be expected followed by a velocity decrease (through lowering of the effective stress) [Grêt et al. 2006; Caudron et al. 2015]. It is therefore difficult to explain either a velocity increase close to the crater terrace—where high temperatures are observed [Revil et al. 2023]—or a velocity decrease at other parts of the edifice where temperatures are much lower [Revil et al. 2023]. Thus we do not consider a change in the proportion of gas a likely mechanism to explain the observed velocity changes.

These observations highlight the challenges in interpreting seismic velocity changes in volcanic regions, where the style of change can be highly variable in different locations on the edifice. We consider that increases in magma overpressure provide the most likely explanation for velocity decreases at lower frequencies. The observation of increasing velocities at STRA station relative to other stations may be explained by a local response to the same source within the vicinity of the crater terrace. Following this, the subsequent decreases relative to other stations following major eruptive events—such as the 2014 flank eruption and 2019 paroxysms—could represent a release of pressure within the upper part of the conduit. This interpretation should, however, clearly be explored in further detail, ideally with the use of modeling that can capture varied behaviour over different parts of the edifice.

An interesting observation is that the difference between velocities at STRA station and the other stations remains at approximately zero, or lower, following the 2019 paroxysms. This is despite significant volcanic activity continuing, with a further paroxysm recorded mid-2020 (albeit much smaller than the 2019 paroxysms) [Calvari et al. 2021]. Similarly, CO_2 flux remained high following the 2019 paroxysms, with further increases from mid-2020 [Inguaggiato et al. 2021]. This therefore contrasts with the 2017–2019 time period, where heightened activity resulted in higher relative velocities at STRA station. We interpret that this relates to significant changes in the shallow plumbing system following the 2019 paroxysms. This is evidenced by significant decreases in velocity and corresponding correlation coefficients above 1 Hz following the first paroxysm in July (largest in the 1–2 Hz range, Figure 2B). Thus, we interpret that the 2019 paroxysms damaged the shallow conduit, with consistent activity over the years following preventing the volcano returning to a 'background' state. This can also explain the lack of a significant velocity decrease associated with both the August 2019 and July 2020 paroxysms, as the system was already damaged. This observation is similar to velocity changes observed at Whakaari volcano, where only the first of two tectonic earthquakes in late 2016 induced a velocity decrease despite the second having stronger ground shaking [Yates et al. 2019]. In contrast, the results at 0.5–1.0 Hz (Figure 2A) do not suggest large structural changes due to the paroxysms. Thus, we consider that the deeper portion of the volcanic conduit (approximately 400–1000 m) was not significantly damaged by the paroxysms. The low velocities that continue through 2020–2022 (Figure 4) could then reflect the continued input of CO_2-rich volatiles that drive more significant eruptive activity during this time period. This may also explain more extreme values in low frequency velocities recorded by some individual stations (e.g. STRE, IST3; Supplementary Material 1 Figure S10A) and station-pairs (e.g. STRA–STRE; Supplementary Material 1 Figure S10B). However, we exercise caution interpreting these specific changes without more detailed analysis to verify their reliability, instead choosing to focus on changes prior to the 2019 paroxysms.

4.4 Implications for monitoring

The results of this study highlight how coda wave interferometry can be a useful complementary tool towards monitoring the state of open-conduit volcanoes. By examining the relative difference in velocities at the summit station (STRA), closest to the crater terrace, clear changes were revealed consistent with previous observations of unrest in the years preceding the 2019 paroxysms (e.g. increased CO_2 flux, VLP occurence, tremor). Similarly, a long-term velocity decrease was observed at lower frequencies in the build-up to the 2019 paroxysms. These changes are thought to reflect the interaction of the shallow plumbing system to increased volatile input at depth.

It is of interest that the largest difference in seismic velocities (2–4 Hz) recorded between STRA station and the other four stations occurs in the month prior to the July 2019 paroxysm. Similarly, the lowest velocities recorded at lower frequencies (0.5–1.0 Hz) using station-pair results—found to be less sensitive to seasonal changes—were between January and July 2019. It is widely agreed that paroxysms result from the fast ascent and injection of deeply stored volatile fluids (2–10 days prior) from the deeper LP storage system (7–10 km) into the shallow plumbing system (2–4 km) [Métrich et al. 2021; Voloschina et al. 2023]. For this reason it is not anticipated that seismic velocity changes are sensitive to this process. How-

ever, changes in the shallow volcanic system could still be useful towards monitoring the likelihood of more dangerous events. For example, increased pressurization within the shallow volcanic system towards more critical values may indicate greater disequilibrium in the input and output of CO_2 rich gas at depth [Inguaggiato et al. 2019; 2020; Aiuppa et al. 2021]. Maximum differences in the velocities recorded at STRA station in the months prior to the 2019 paroxysms may then be a reflection of a deeper plumbing system that is becoming increasingly unstable. However, it is unclear how much of a role this plays in the eventual triggering of the 2019 paroxysm, where it has also been suggested a blockage within the shallow conduit only a few minutes before the event may have been the triggering process [Viccaro et al. 2021].

Finally, the detection of an anomalous velocity change in the shallow subsurface only by relative comparison between the station closest to the crater terrace with the other stations has important implications for monitoring shallow changes. Seasonal changes dominated the velocity changes above 1 Hz at all stations, with amplitudes of approximately ±0.5 %. In comparison, the relative differences measured at STRA station—compared to other stations—varied by approximately ±0.2 %. Thus, it remains a challenge to distinguish volcanic changes from seasonal processes, with the identification of an anomalous signal possible here only with the use of a station approximately 500 m from the crater terrace. These findings suggest two things towards monitoring volcanoes with coda wave interferometry: (1) the need for better tools for correcting seasonal trends and (2) the need for stations close to active vents in order to detect subtle changes within the shallow plumbing system. This will greatly improve the ability to detect anomalous behavior that could suggest an increased probability of major events at the volcano.

5 Conclusions

Coda wave interferometry was applied towards the goal of computing seismic velocity changes over a nine-year period at Stromboli, encompassing various styles of volcanic activity. Particular attention is given to two paroxysms in 2019, which occurred with minimal warning approximately two months apart.

Velocity changes were computed in three frequency bands (0.5–1.0 Hz, 1.0–2.0 Hz, and 2.0–4.0 Hz), between pairs of seismic stations and also between components of individual single seismic stations. Results were comparable between both datasets, with seasonal processes dominating the velocity changes (especially above 1 Hz) with amplitudes of approximately ±0.5 %. Precipitation-induced changes are considered the most likely contributing process, though temperature-induced changes cannot be ruled out. Two key features of interest are identified that are not readily explained by a seasonal process. The first feature is a long-term velocity decrease from early 2017 at lower frequencies (0.5–1.0 Hz), reaching a minimum in early 2019. Lower velocities are also recorded prior to the 2014 flank eruption and following the 2019 paroxysms. The second feature is an increasing velocity at the station closest to the summit (STRA) relative to the other stations at higher frequencies (primarily 2–4 Hz). This increasing trend begins in 2017 and reaches a maximum approximately one month before the July 3 paroxysm. Post-paroxysm, the difference between STRA station and other stations returns to approximately zero, considered to reflect a decrease of pressures within the shallow plumbing system. Notably, this difference remains at zero despite ongoing eruptive activity, which—combined with significant decreases in seismic velocities and corresponding correlation coefficients following the 2019 paroxysms—suggests lasting damage to the shallow conduit. In contrast, at lower frequencies, velocities remain relatively low through 2020 and 2021, with no significant structural damage inferred. Low velocities through this time period may therefore reflect continued volatile input that sustains elevated eruptive activity.

The long-term velocity decreases at lower frequencies from early 2017, combined with the increasing velocity at STRA station (relative to other stations) at higher frequencies, are aligned with previous observations of increasing activity during the same time period. This is thought to reflect the response of the shallow volcanic system to increased volatile input following the injection of new CO_2-rich magmatic fluids into the deeper storage zone. We consider that increases in magma overpressure in response to the input of new volatiles provides the most likely explanation for velocity decreases at lower frequencies. The increasing velocity at STRA station relative to other stations is thought to be due to a local response to the same pressure source within the vicinity of the crater terrace. However, we suggest that this interpretation should be further explored.

The results highlight how coda wave interferometry can be a useful complementary tool towards monitoring the state of open-conduit volcanoes. While sensitivity to deeper magma storage zones is not expected, increased pressurization within the shallow volcanic system towards more critical values may reflect an increasingly unstable deeper plumbing system. Thus, monitoring seismic velocity changes may be useful towards anticipating the likelihood of significant volcanic events while enhancing our understanding of the subsurface changes that precede such episodes.

Author Contributions

AY, CC, AM, and PL contributed to the conception and design of the study. AY, AC, FC and TL contributed to preparation of seismic datasets. AY performed all processing of seismic and meteorological datasets. AM and TL aided in the preparation of codes used for computing sensitivity kernels. All authors contributed to the interpretation of results. Manuscript (text and figures) prepared by AY, with all authors contributing to manuscript revisions prior to submission.

Acknowledgements

A. Yates was supported by funding from the Ministère de l'Enseignement supérieur, de la Recherche et de l'Innovation (MESRI). The `Python` package `MSNoise` [Lecocq et al. 2014] was used to process raw data through to velocity changes. 1D sensitivity kernels were prepared using modified codes of Haney and Tsai [2017] (https://github.com/matt-haney/raylee_codes). Finally, we thank Editor Dr Emma Nichol-

son and the reviewers (Dr Alicia Hotovec-Ellis and one anonymous reviewer) for their comments towards an improved manuscript.

Data Availability

Seismic data for stations IST3 and ISTR stations are publicly available via the INGV Seismological Data Center [INGV Data Center 2006]. Seismic data for stations STR1, STRA, and STRE are available upon request to the INGV, Osservatorio Etneo. All velocity changes presented using the stretching technique, both averaged and individually, are available in Supplementary Material 2. Specific parameter choices used in `MSNoise` are also included in Supplementary Material 1 (Tables S1 and S2). Meteorological data are publicly available from the Global Surface Summary of the Day (GSOD) dataset [National Climate Data Center 2013].

Copyright notice

References

Aiuppa, A., A. Bertagnini, N. Métrich, R. Moretti, A. Di Muro, M. Liuzzo, and G. Tamburello (2010). "A model of degassing for Stromboli volcano". *Earth and Planetary Science Letters* 295(1-2), pages 195–204. DOI: 10.1016/j.epsl.2010.03.040.

Aiuppa, A., M. Burton, P. Allard, T. Caltabiano, G. Giudice, S. Gurrieri, M. Liuzzo, and G. Salerno (2011). "First observational evidence for the CO2-driven origin of Stromboli's major explosions". *Solid Earth* 2(2), pages 135–142. DOI: 10.5194/se-2-135-2011.

Aiuppa, A., M. Bitetto, D. D. Donne, F. P. la Monica, G. Tamburello, D. Coppola, M. D. Schiava, L. Innocenti, G. Lacanna, M. Laiolo, F. Massimetti, M. Pistolesi, M. C. Silengo, and M. Ripepe (2021). "Volcanic CO2 tracks the incubation period of basaltic paroxysms". *Science Advances* 7(38). DOI: 10.1126/sciadv.abh0191.

Allard, P. (2010). "A CO2-rich gas trigger of explosive paroxysms at Stromboli basaltic volcano, Italy". *Journal of Volcanology and Geothermal Research* 189(3-4), pages 363–374. DOI: 10.1016/j.jvolgeores.2009.11.018.

Andajani, R. D., T. Tsuji, R. Snieder, and T. Ikeda (2020). "Spatial and temporal influence of rainfall on crustal pore pressure based on seismic velocity monitoring". *Earth, Planets and Space* 72(1). DOI: 10.1186/s40623-020-01311-1.

Andronico, D., E. Del Bello, C. D'Oriano, P. Landi, F. Pardini, P. Scarlato, M. de' Michieli Vitturi, J. Taddeucci, A. Cristaldi, F. Ciancitto, F. Pennacchia, T. Ricci, and F. Valentini (2021). "Uncovering the eruptive patterns of the 2019 double paroxysm eruption crisis of Stromboli volcano". *Nature Communications* 12(1), pages 1–14. DOI: 10.1038/s41467-021-24420-1.

Apuani, T. and C. Corazzato (2009). "Numerical model of the Stromboli volcano (Italy) including the effect of magma pressure in the dyke system". *Rock Mechanics and Rock Engineering* 42(1), pages 53–72. DOI: 10.1007/s00603-008-0163-1.

Barberi, F., L. Civetta, P. Gasparini, F. Innocenti, R. Scandone, and L. Villari (1974). "Evolution of a section of the Africa-Europe plate boundary: Paleomagnetic and volcanological evidence from Sicily". *Earth and Planetary Science Letters* 22(2), pages 123–132. DOI: 10.1016/0012-821X(74)90072-7.

Belien, I. B., K. V. Cashman, and A. W. Rempel (2010). "Gas accumulation in particle-rich suspensions and implications for bubble populations in crystal-rich magma". *Earth and Planetary Science Letters* 297(1-2), pages 133–140. DOI: 10.1016/j.epsl.2010.06.014.

Ben-Zion, Y. and P. Leary (1986). "Thermoelastic strain in a half-space covered by unconsolidated material". *Bulletin of the Seismological Society of America* 76(5), pages 1447–1460.

Bennington, N. L., M. Haney, S. De Angelis, C. H. Thurber, and J. Freymueller (2015). "Monitoring changes in seismic velocity related to an ongoing rapid inflation event at Okmok volcano, Alaska". *Journal of Geophysical Research: Solid Earth* 120(8), pages 5664–5676. DOI: 10.1002/2015JB011939.

Bosman, A., F. L. Chiocci, and C. Romagnoli (2009). "Morphostructural setting of Stromboli volcano revealed by high-resolution bathymetry and backscatter data of its submarine portions". *Bulletin of Volcanology* 71(9), pages 1007–1019. DOI: 10.1007/s00445-009-0279-5.

Brenguier, F., M. Campillo, T. Takeda, Y. Aoki, N. M. Shapiro, X. Briand, K. Emoto, and H. Miyake (2014). "Mapping pressurized volcanic fluids from induced crustal seismic velocity drops". *Science* 345(6192), pages 80–82. DOI: 10.1126/science.1254073.

Brenguier, F., N. M. Shapiro, M. Campillo, V. Ferrazzini, Z. Duputel, O. Coutant, and A. Nercessian (2008). "Towards forecasting volcanic eruptions using seismic noise". *Nature Geoscience* 1(2), pages 126–130. DOI: 10.1038/ngeo104.

Budi-Santoso, A. and P. Lesage (2016). "Velocity variations associated with the large 2010 eruption ofMerapi volcano, Java, retrieved from seismic multiplets and ambient noise cross-correlation". *Geophysical Journal International* 206(1), pages 221–240. DOI: 10.1093/gji/ggw145.

Burton, M., P. Allard, F. Mure, and A. La Spina (2007). "Magmatic gas composition reveals the source depth of slug-driven strombolian explosive activity". *Science* 317(5835), pages 227–230. DOI: 10.1126/science.1141900.

Calò, M., E. A. López Mazariegos, A. Tramelli, and M. Orazi (2021). "Hydrothermal systems characterization of the Stromboli volcano using spatial and temporal changes of the seismic velocities". *Journal of Volcanology and Geothermal Research* 411. DOI: 10.1016/j.jvolgeores.2021.107177.

Calvari, S., F. Di Traglia, G. Ganci, V. Bruno, F. Ciancitto, B. Di Lieto, S. Gambino, A. Garcia, F. Giudicepietro, S. Inguaggiato, F. Vita, M. Cangemi, C. Inguaggiato, G. Macedonio, M.

Mattia, L. Miraglia, T. Nolesini, M. Pompilio, P. Romano, G. Salerno, N. Casagli, G. Re, P. Del Carlo, A. Di Roberto, A. Cappello, C. Corradino, E. Amato, F. Torrisi, C. Del Negro, A. M. Esposito, W. De Cesare, T. Caputo, M. F. Buongiorno, M. Musacchio, V. Romaniello, M. Silvestri, E. Marotta, R. Avino, G. Avvisati, and P. Belviso (2022). "Multi-parametric study of an eruptive phase comprising unrest, major explosions, crater failure, pyroclastic density currents and lava flows: Stromboli volcano, 1 December 2020–30 June 2021". *Frontiers in Earth Science* 10(August 2019), pages 1–24. DOI: 10.3389/feart.2022.899635.

Calvari, S., F. Giudicepietro, F. Di Traglia, A. Bonaccorso, G. Macedonio, and N. Casagli (2021). "Variable magnitude and intensity of strombolian explosions: Focus on the eruptive processes for a first classification scheme for stromboli volcano (italy)". *Remote Sensing* 13(5), pages 1–30. DOI: 10.3390/rs13050944.

Casagli, N., A. Tibaldi, A. Merri, C. Del Ventisette, T. Apuani, L. Guerri, J. Fortuny-Guasch, and D. Tarchi (2009). "Deformation of Stromboli Volcano (Italy) during the 2007 eruption revealed by radar interferometry, numerical modelling and structural geological field data". *Journal of Volcanology and Geothermal Research* 182(3-4), pages 182–200. DOI: 10.1016/j.jvolgeores.2009.01.002.

Caudron, C., Y. Aoki, T. Lecocq, R. De Plaen, J. Soubestre, A. Mordret, L. Seydoux, and T. Terakawa (2022). "Hidden pressurized fluids prior to the 2014 phreatic eruption at Mt Ontake". *Nature Communications* 13(1), pages 1–9. DOI: 10.1038/s41467-022-32252-w.

Caudron, C., T. Girona, A. Jolly, B. Christenson, M. K. Savage, R. Carniel, T. Lecocq, B. Kennedy, I. Lokmer, A. Yates, I. Hamling, I. Park, G. Kilgour, and A. Mazot (2021). "A quest for unrest in multiparameter observations at Whakaari/White Island volcano, New Zealand 2007–2018". *Earth, Planets and Space* 73(1). DOI: 10.1186/s40623-021-01506-0.

Caudron, C., T. Lecocq, D. K. Syahbana, W. McCausland, A. Watlet, T. Camelbeeck, A. Bernard, and Surono (2015). "Stress and mass changes at a "wet" volcano: Example during the 2011-2012 volcanic unrest at Kawah Ijen volcano (Indonesia)". *Journal of Geophysical Research: Solid Earth* 120(7), pages 5117–5134. DOI: 10.1002/2014JB011590.

Chouet, B., G. De Luca, G. Milana, P. Dawson, M. Martini, and R. Scarpa (1998). "Shallow velocity structure of Stromboli Volcano, Italy, derived from small-aperture array measurements of Strombolian tremor". *Bulletin of the Seismological Society of America* 88(3), pages 653–666. DOI: 10.1785/bssa0880030653.

Clarke, D., L. Zaccarelli, N. M. Shapiro, and F. Brenguier (2011). "Assessment of resolution and accuracy of the Moving Window Cross Spectral technique for monitoring crustal temporal variations using ambient seismic noise". *Geophysical Journal International* 186(2), pages 867–882. DOI: 10.1111/j.1365-246X.2011.05074.x.

Clarke, J., L. Adam, K. van Wijk, and J. Sarout (2020). "The influence of fluid type on elastic wave velocity and attenuation in volcanic rocks". *Journal of Volcanology and Geothermal Research* 403. DOI: 10.1016/j.jvolgeores.2020.107004.

Clements, T. and M. A. Denolle (2018). "Tracking Groundwater Levels Using the Ambient Seismic Field". *Geophysical Research Letters* 45(13), pages 6459–6465. DOI: 10.1029/2018GL077706.

Cubuk-Sabuncu, Y., K. Jónsdóttir, C. Caudron, T. Lecocq, M. M. Parks, H. Geirsson, and A. Mordret (2021). "Temporal Seismic Velocity Changes During the 2020 Rapid Inflation at Mt. Þorbjörn-Svartsengi, Iceland, Using Seismic Ambient Noise". *Geophysical Research Letters* 48(11), pages 1–10. DOI: 10.1029/2020GL092265.

De Plaen, R. S., A. Cannata, F. Cannavo', C. Caudron, T. Lecocq, and O. Francis (2019). "Temporal changes of seismic velocity caused by volcanic activity at Mt. Etna revealed by the autocorrelation of ambient seismic noise". *Frontiers in Earth Science* 6(January), pages 1–11. DOI: 10.3389/feart.2018.00251.

Di Lieto, B., P. Romano, R. Scarpa, and A. T. Linde (2020). "Strain Signals Before and During Paroxysmal Activity at Stromboli Volcano, Italy". *Geophysical Research Letters* 47(21). DOI: 10.1029/2020GL088521.

Di Traglia, F., M. Battaglia, T. Nolesini, D. Lagomarsino, and N. Casagli (2015). "Shifts in the eruptive styles at Stromboli in 2010-2014 revealed by ground-based InSAR data". *Scientific Reports* 5, pages 1–11. DOI: 10.1038/srep13569.

Di Traglia, F., S. Calvari, L. D'Auria, T. Nolesini, A. Bonaccorso, A. Fornaciai, A. Esposito, A. Cristaldi, M. Favalli, and N. Casagli (2018). "The 2014 effusive eruption at stromboli: New insights from in situ and remote-sensing measurements". *Remote Sensing* 10(12). DOI: 10.3390/rs10122035.

Di Traglia, F., C. De Luca, M. Manzo, T. Nolesini, N. Casagli, R. Lanari, and F. Casu (2021). "Joint exploitation of space-borne and ground-based multitemporal InSAR measurements for volcano monitoring: The Stromboli volcano case study". *Remote Sensing of Environment* 260(March), page 112441. DOI: 10.1016/j.rse.2021.112441.

Di Traglia, F., C. Del Ventisette, M. Rosi, F. Mugnai, E. Intrieri, S. Moretti, and N. Casagli (2013). "Ground-based InSAR reveals conduit pressurization pulses at Stromboli volcano". *Terra Nova* 25(3), pages 192–198. DOI: 10.1111/ter.12020.

Di Traglia, F., T. Nolesini, E. Intrieri, F. Mugnai, D. Leva, M. Rosi, and N. Casagli (2014). "Review of ten years of volcano deformations recorded by the ground-based InSAR monitoring system at Stromboli volcano: A tool to mitigate volcano flank dynamics and intense volcanic activity". *Earth-Science Reviews* 139, pages 317–335. DOI: 10.1016/j.earscirev.2014.09.011.

Donaldson, C., C. Caudron, R. G. Green, W. A. Thelen, and R. S. White (2017). "Relative seismic velocity variations correlate with deformation at Kīlauea volcano". *Science Advances* 3(6), e1700219. DOI: 10.1126/sciadv.1700219.

Duputel, Z., V. Ferrazzini, F. Brenguier, N. Shapiro, M. Campillo, and A. Nercessian (2009). "Real time monitoring of relative velocity changes using ambient seismic noise at the Piton de la Fournaise volcano (La Réunion) from January 2006 to June 2007". *Journal of Volcanology and*

Geothermal Research 184(1-2), pages 164–173. DOI: 10.1016/j.jvolgeores.2008.11.024.

Edmonds, M., E. J. Liu, and K. V. Cashman (2022). "Open-vent volcanoes fuelled by depth-integrated magma degassing". *Bulletin of Volcanology* 84(3). DOI: 10.1007/s00445-021-01522-8.

Federico, C., S. Inguaggiato, M. Liotta, A. L. Rizzo, and F. Vita (2023). "Decadal Monitoring of the Hydrothermal System of Stromboli Volcano, Italy". *Geochemistry, Geophysics, Geosystems* 24(9). DOI: 10.1029/2023GC010931.

Feng, K. F., H. H. Huang, Y. J. Hsu, and Y. M. Wu (2021). "Controls on Seasonal Variations of Crustal Seismic Velocity in Taiwan Using Single-Station Cross-Component Analysis of Ambient Noise Interferometry". *Journal of Geophysical Research: Solid Earth* 126(11). DOI: 10.1029/2021JB022650.

Finizola, A., M. Aubert, A. Revil, C. Schütze, and F. Sortino (2009). "Importance of structural history in the summit area of Stromboli during the 2002-2003 eruptive crisis inferred from temperature, soil CO2, self-potential, and electrical resistivity tomography". *Journal of Volcanology and Geothermal Research* 183(3-4), pages 213–227. DOI: 10.1016/j.jvolgeores.2009.04.002.

Finizola, A., F. Sortino, J. F. Lénat, and M. Valenza (2002). "Fluid circulation at Stromboli volcano (Aeolian Islands, Italy) from self-potential and CO2 surveys". *Journal of Volcanology and Geothermal Research* 116(1-2), pages 1–18. DOI: 10.1016/S0377-0273(01)00327-4.

Francalanci, L., S. Tommasini, and S. Conticelli (2004). "The volcanic activity of Stromboli in the 1906-1998 AD period: Mineralogical, geochemical and isotope data relevant to the understanding of the plumbing system". *Journal of Volcanology and Geothermal Research* 131(1-2), pages 179–211. DOI: 10.1016/S0377-0273(03)00362-7.

Giudicepietro, F., S. Calvari, S. Alparone, F. Bianco, A. Bonaccorso, V. Bruno, T. Caputo, A. Cristaldi, L. D'Auria, W. D. Cesare, B. D. Lieto, A. M. Esposito, S. Gambino, S. Inguaggiato, G. Macedonio, M. Martini, M. Mattia, M. Orazi, A. Paonita, R. Peluso, E. Privitera, P. Romano, G. Scarpato, A. Tramelli, and F. Vita (2019). "Integration of ground-based remote-sensing and in situ multidisciplinary monitoring data to analyze the eruptive activity of stromboli volcano in 2017-2018". *Remote Sensing* 11(15). DOI: 10.3390/rs11151813.

Giudicepietro, F., C. López, G. Macedonio, S. Alparone, F. Bianco, S. Calvari, W. De Cesare, D. Delle Donne, B. Di Lieto, A. M. Esposito, M. Orazi, R. Peluso, E. Privitera, P. Romano, G. Scarpato, and A. Tramelli (2020). "Geophysical precursors of the July-August 2019 paroxysmal eruptive phase and their implications for Stromboli volcano (Italy) monitoring". *Scientific Reports* 10(1), pages 1–16. DOI: 10.1038/s41598-020-67220-1.

Got, J. L., A. Peltier, T. Staudacher, P. Kowalski, and P. Boissier (2013). "Edifice strength and magma transfer modulation at Piton de la Fournaise volcano". *Journal of Geophysical Research: Solid Earth* 118(9), pages 5040–5057. DOI: 10.1002/jgrb.50350.

Grêt, A., R. Snieder, and J. Scales (2006). "Time-lapse monitoring of rock properties with coda wave interferometry". *Journal of Geophysical Research: Solid Earth* 111(3), pages 1–11. DOI: 10.1029/2004JB003354.

Haney, M. M. and V. C. Tsai (2017). "Perturbational and nonperturbational inversion of Rayleigh-wave velocities". *Geophysics* 82(3), F15–F28. DOI: 10.1190/GEO2016-0397.1.

Harris, A. and M. Ripepe (2007). "Temperature and dynamics of degassing at Stromboli". *Journal of Geophysical Research: Solid Earth* 112(3), pages 1–18. DOI: 10.1029/2006JB004393.

Hillers, G., Y. Ben-Zion, M. Campillo, and D. Zigone (2015a). "Seasonal variations of seismic velocities in the San Jacinto fault area observed with ambient seismic noise". *Geophysical Journal International* 202(2), pages 920–932. DOI: 10.1093/gji/ggv151.

Hillers, G., S. Husen, A. Obermann, T. Planès, E. Larose, and M. Campillo (2015b). "Noise-based monitoring and imaging of aseismic transient deformation induced by the 2006 Basel reservoir stimulation". *Geophysics* 80(4), KS51–KS68. DOI: 10.1190/geo2014-0455.1.

Hotovec-Ellis, A. J., J. Gomberg, J. E. Vidale, and K. C. Creager (2014). "A continuous record of intereruption velocity change at Mount St. Helens from coda wave interferometry". *Journal of Geophysical Research: Solid Earth* 119(3), pages 2199–2214. DOI: 10.1002/2013JB010742.

Hotovec-Ellis, A. J., B. R. Shiro, D. R. Shelly, K. R. Anderson, M. M. Haney, W. A. Thelen, E. K. Montgomery-Brown, and I. A. Johanson (2022). "Earthquake-Derived Seismic Velocity Changes During the 2018 Caldera Collapse of Kīlauea Volcano". *Journal of Geophysical Research: Solid Earth* 127(2). DOI: 10.1029/2021JB023324.

Inguaggiato, S., F. Vita, M. Cangemi, and L. Calderone (2019). "Increasing summit degassing at the stromboli volcano and relationships with volcanic activity (2016-2018)". *Geosciences (Switzerland)* 9(4). DOI: 10.3390/geosciences9040176.

– (2020). "Changes in CO2 soil degassing style as a possible precursor to volcanic activity: The 2019 case of Stromboli paroxysmal eruptions". *Applied Sciences (Switzerland)* 10(14). DOI: 10.3390/app10144757.

Inguaggiato, S., F. Vita, M. Cangemi, C. Inguaggiato, and L. Calderone (2021). "The monitoring of CO2 soil degassing as indicator of increasing volcanic activity: The paroxysmal activity at stromboli volcano in 2019-2021". *Geosciences (Switzerland)* 11(4). DOI: 10.3390/geosciences11040169.

Inguaggiato, S., F. Vita, M. Cangemi, A. Mazot, A. Sollami, L. Calderone, S. Morici, and M. P. Jacome Paz (2017). "Stromboli volcanic activity variations inferred from observations of fluid geochemistry: 16 years of continuous monitoring of soil CO2 fluxes (2000–2015)". *Chemical Geology* 469, pages 69–84. DOI: 10.1016/j.chemgeo.2017.01.030.

Inguaggiato, S., F. Vita, D. Rouwet, N. Bobrowski, S. Morici, and A. Sollami (2011). "Geochemical evidence of the renewal of volcanic activity inferred from CO2 soil and SO2 plume fluxes: The 2007 Stromboli eruption (Italy)". *Bulletin of Volcanology* 73(4), pages 443–456. DOI: 10.1007/s00445-010-0442-z.

INGV Data Center (2006). *INGV Seismological Data Centre, Rete Sismica Nazionale (RSN). Italy: Istituto Nazionale di Geofisica e Vulcanologia (INGV). https://eida.ingv.it/en/network/IV*. DOI: https://doi.org/10.13127/SD/X0FXNH7QFY.

Iverson, R. M. (1995). "Can magma-injection and groundwater forces cause massive landslides on Hawaiian volcanoes?" *Journal of Volcanology and Geothermal Research* 66(1-4), pages 295–308. DOI: 10.1016/0377-0273(94)00064-N.

Iwasaki, I., T. Ozawa, M. Yoshida, T. Katsura, B. Iwasaki, and M. Kamada (1962). "Chemical composition of volcanic gases in Japan". *Bulletin Volcanologique* 24(1), pages 23–48. DOI: 10.1007/BF02599327.

Landi, P., N. Métrich, A. Bertagnini, and M. Rosi (2004). "Dynamics of magma mixing and degassing recorded in plagioclase at Stromboli (Aeolian Archipelago, Italy)". *Contributions to Mineralogy and Petrology* 147(2), pages 213–227. DOI: 10.1007/s00410-004-0555-5.

Lecocq, T., C. Caudron, and F. Brenguier (2014). "Msnoise, a python package for monitoring seismic velocity changes using ambient seismic noise". *Seismological Research Letters* 85(3), pages 715–726. DOI: 10.1785/0220130073.

Lecocq, T., L. Longuevergne, H. A. Pedersen, F. Brenguier, and K. Stammler (2017). "Monitoring ground water storage at mesoscale using seismic noise: 30 years of continuous observation and thermo-elastic and hydrological modeling". *Scientific Reports* 7(1), page 14241. DOI: 10.1038/s41598-017-14468-9.

Lockner, D. A., J. B. Walsh, and J. D. Byerlee (1977). "Changes in seismic velocity and attenuation during deformation of granite". *Journal of Geophysical Research* 82(33), pages 5374–5378. DOI: 10.1029/jb082i033p05374.

Lumley, D. (2010). "4D seismic monitoring of CO2 sequestration". *ASEG Extended Abstracts* 2010(1), pages 1–4. DOI: 10.1081/22020586.2010.12041906.

Machacca-Puma, R., P. Lesage, E. Larose, P. Lacroix, and R. M. Anccasi-Figueroa (2019). "Detection of pre-eruptive seismic velocity variations at an andesitic volcano using ambient noise correlation on 3-component stations: Ubinas volcano, Peru, 2014". *Journal of Volcanology and Geothermal Research* 381, pages 83–100. DOI: 10.1016/j.jvolgeores.2019.05.014.

Makus, P., C. Sens-Schönfelder, L. Illien, T. R. Walter, A. Yates, and F. Tilmann (2023). "Deciphering the Whisper of Volcanoes: Monitoring Velocity Changes at Kamchatka's Klyuchevskoy Group With Fluctuating Noise Fields". *Journal of Geophysical Research: Solid Earth* 128(4). DOI: 10.1029/2022JB025738.

Mao, S., A. Mordret, M. Campillo, H. Fang, and R. D. van der Hilst (2020). "On the measurement of seismic traveltime changes in the time-frequency domain with wavelet cross-spectrum analysis". *Geophysical Journal International* 221(1), pages 550–568. DOI: 10.1093/gji/ggz495.

McKee, K. F., D. C. Roman, G. P. Waite, and D. Fee (2022). "Silent Very Long Period Seismic Events (VLPs) at Stromboli Volcano, Italy". *Geophysical Research Letters* 49(23). DOI: 10.1029/2022GL100735.

McTigue, D. F. (1987). "Elastic stress and deformation near a finite spherical magma body: Resolution of the point source paradox". *Journal of Geophysical Research: Solid Earth* 92(B12), pages 12931–12940. DOI: 10.1029/jb092ib12p12931.

Meier, U., N. M. Shapiro, and F. Brenguier (2010). "Detecting seasonal variations in seismic velocities within Los Angeles basin from correlations of ambient seismic noise". *Geophysical Journal International* 181(2), pages 985–996. DOI: 10.1111/j.1365-246X.2010.04550.x.

Métrich, N., A. Bertagnini, and A. Di Muro (2009). "Conditions of magma storage, degassing and ascent at Stromboli: New insights into the volcano plumbing system with inferences on the eruptive dynamics". *Journal of Petrology* 51(3), pages 603–626. DOI: 10.1093/petrology/egp083.

Métrich, N., A. Bertagnini, P. Landi, and M. Rosi (2001). "Crystallization driven by decompression and water loss at Stromboli volcano (Aeolian Islands, Italy)". *Journal of Petrology* 42(8), pages 1471–1490. DOI: 10.1093/petrology/42.8.1471.

Métrich, N., A. Bertagnini, P. Landi, M. Rosi, and O. Belhadj (2005). "Triggering mechanism at the origin of paroxysms at Stromboli (Aeolian Archipelago, Italy): The 5 April 2003 eruption". *Geophysical Research Letters* 32(10), pages 1–4. DOI: 10.1029/2004GL022257.

Métrich, N., A. Bertagnini, and M. Pistolesi (2021). "Paroxysms at Stromboli Volcano (Italy): Source, Genesis and Dynamics". *Frontiers in Earth Science* 9(February), pages 1–17. DOI: 10.3389/feart.2021.593339.

Mordret, A., A. D. Jolly, Z. Duputel, and N. Fournier (2010). "Monitoring of phreatic eruptions using Interferometry on Retrieved Cross-Correlation Function from Ambient Seismic Noise: Results from Mt. Ruapehu, New Zealand". *Journal of Volcanology and Geothermal Research* 191(1-2), pages 46–59. DOI: 10.1016/j.jvolgeores.2010.01.010.

Muzellec, T., P. Lesage, C. Caudron, and J. L. Got (2023). "Migration of Mechanical Perturbations Estimated by Seismic Coda Wave Interferometry During the 2018 Pre-Eruptive Period at Kīlauea Volcano, Hawaii". *Journal of Geophysical Research: Solid Earth* 128(8). DOI: 10.1029/2022JB026224.

National Climate Data Center (2013). *Global Surface Summary of the Day. (http://www.ncdc.noaa.gov/)*.

Niu, F., P. G. Silver, T. M. Daley, X. Cheng, and E. L. Majer (2008). "Preseismic velocity changes observed from active source monitoring at the Parkfield SAFOD drill site". *Nature* 454(7201), pages 204–208. DOI: 10.1038/nature07111.

Nur, A. (1971). "Effects of stress on velocity anisotropy in rocks with cracks". *Journal of Geophysical Research* 76(8), pages 2022–2034. DOI: 10.1029/jb076i008p02022.

Nur, A. and G. Simmons (1969). "Stress-Induced Velocity Anisotropy in Rock. an Experimental Study". *J Geophys Res* 74(27), pages 6667–6674. DOI: 10.1029/jb074i027p06667.

Obermann, A., T. Planès, E. Larose, and M. Campillo (2013). "Imaging preeruptive and coeruptive structural and mechanical changes of a volcano with ambient seismic noise". *Journal of Geophysical Research: Solid Earth* 118(12), pages 6285–6294. DOI: 10.1002/2013JB010399.

Oppenheimer, J., A. Capponi, K. V. Cashman, S. J. Lane, A. C. Rust, and M. R. James (2020). "Analogue experiments on the rise of large bubbles through a solids-rich suspension: A "weak plug" model for Strombolian eruptions". *Earth and Planetary Science Letters* 531, page 115931. DOI: 10.1016/j.epsl.2019.115931.

Oppenheimer, J., A. C. Rust, K. V. Cashman, and B. Sandnes (2015). "Gas migration regimes and outgassing in particle-rich suspensions". *Frontiers in Physics* 3(AUG), pages 1–13. DOI: 10.3389/fphy.2015.00060.

Paasschens, J. C. (1997). "Solution of the time-dependent Boltzmann equation". *Physical Review E - Statistical Physics, Plasmas, Fluids, and Related Interdisciplinary Topics* 56(1), pages 1135–1141. DOI: 10.1103/PhysRevE.56.1135.

Pacheco, C. and R. Snieder (2005). "Time-lapse travel time change of multiply scattered acoustic waves". *The Journal of the Acoustical Society of America* 118(3), pages 1300–1310. DOI: 10.1121/1.2000827.

Planès, T., E. Larose, L. Margerin, V. Rossetto, and C. Sens-Schönfelder (2014). "Decorrelation and phase-shift of coda waves induced by local changes: Multiple scattering approach and numerical validation". *Waves in Random and Complex Media* 24(2), pages 99–125. DOI: 10.1080/17455030.2014.880821.

Poupinet, G., W. L. Ellsworth, and J. Frechet (1984). "Monitoring velocity variations in the crust using earthquake doublets: an application to the Calaveras fault, California (USA)." *Journal of Geophysical Research* 89(B7), pages 5719–5731. DOI: 10.1029/JB089iB07p05719.

Prudencio, J., E. Del Pezzo, J. M. Ibáñez, E. Giampiccolo, and D. Patané (2015). "Two-dimensional seismic attenuation images of Stromboli Island using active data". *Geophysical Research Letters* 42(6), pages 1717–1724. DOI: 10.1002/2015GL063293.

Revil, A., A. Finizola, T. Johnson, T. Ricci, M. Gresse, E. Delcher, S. Barde-Cabusson, P. A. Duvillard, and M. Ripepe (2023). "The Thermal Plumbing System of Stromboli Volcano, Aeolian Islands (Italy) Inferred From Electrical Conductivity and Induced Polarization Tomography". *Journal of Geophysical Research: Solid Earth* 128(6). DOI: 10.1029/2023JB026475.

Revil, A., A. Finizola, T. Ricci, E. Delcher, A. Peltier, S. Barde-Cabusson, G. Avard, T. Bailly, L. Bennati, S. Byrdina, J. Colonge, F. Di Gangi, G. Douillet, M. Lupi, J. Letort, and E. Tsang Hin Sun (2011). "Hydrogeology of Stromboli volcano, Aeolian Islands (Italy) from the interpretation of resistivity tomograms, self-potential, soil temperature and soil CO2 concentration measurements". *Geophysical Journal International* 186(3), pages 1078–1094. DOI: 10.1111/j.1365-246X.2011.05112.x.

Revil, A., A. Finizola, F. Sortino, and M. Ripepe (2004). "Geophysical investigations at Stromboli volcano, Italy: Implications for ground water flow and paroxysmal activity". *Geophysical Journal International* 157(1), pages 426–440. DOI: 10.1111/j.1365-246X.2004.02181.x.

Richter, T., C. Sens-Schönfelder, R. Kind, and G. Asch (2014). "Comprehensive observation and modeling of earthquake and temperature-related seismic velocity changes in northern Chile with passive image interferometry". *Journal of Geophysical Research: Solid Earth* 119(6), pages 4747–4765. DOI: 10.1002/2013JB010695.

Ripepe, M., G. Lacanna, M. Pistolesi, M. C. Silengo, A. Aiuppa, M. Laiolo, F. Massimetti, L. Innocenti, M. Della Schiava, M. Bitetto, F. P. La Monica, T. Nishimura, M. Rosi, D. Mangione, A. Ricciardi, R. Genco, D. Coppola, E. Marchetti, and D. Delle Donne (2021). "Ground deformation reveals the scale-invariant conduit dynamics driving explosive basaltic eruptions". *Nature Communications* 12(1), page 1683. DOI: 10.1038/s41467-021-21722-2.

Ripepe, M., D. D. Donne, A. Harris, E. Marchetti, and G. Ulivieri (2013). "Dynamics of Strombolian Activity". *The Stromboli Volcano: An Integrated Study of the 2002-2003 Eruption. (2008)* 182, pages 39–48. DOI: 10.1029/182gm05.

Rivet, D., F. Brenguier, and F. Cappa (2015). "Improved detection of preeruptive seismic velocity drops at the Piton de la Fournaise volcano". *Geophysical Research Letters* 42(15), pages 6332–6339. DOI: 10.1002/2015GL064835.

Rivet, D., F. Brenguier, D. Clarke, N. M. Shapiro, and A. Peltier (2014). "Long-term dynamics of Piton de la Fournaise volcano from 13years of seismic velocity change measurements and GPS observations". *Journal of Geophysical Research: Solid Earth* 119(10), pages 7654–7666. DOI: 10.1002/2014JB011307.

Rizzo, A. L., C. Federico, S. Inguaggiato, A. Sollami, M. Tantillo, F. Vita, S. Bellomo, M. Longo, F. Grassa, and M. Liuzzo (2015). "The 2014 effusive eruption at Stromboli volcano (Italy): Inferences from soil CO2 flux and 3He/4He ratio in thermal waters". *Geophysical Research Letters* 42(7), pages 2235–2243. DOI: 10.1002/2014GL062955.

Rose, W. I., J. L. Palma, H. D. Granados, and N. Varley (2013). "Open-vent volcanism and related hazards: Overview". *Special Paper of the Geological Society of America* 498(November), pages vii–xiii. DOI: 10.1130/2013.2498(00).

Rosi, M., M. Pistolesi, A. Bertagnini, P. Landi, M. Pompilio, and A. Di Roberto (2013). "Stromboli volcano, Aeolian Islands (Italy): Present eruptive activity and hazards". *Geological Society Memoir* 37(1), pages 473–490. DOI: 10.1144/M37.14.

Salvatore, V., A. Silleni, D. Corneli, J. Taddeucci, D. M. Palladino, G. Sottili, D. Bernini, D. Andronico, and A. Cristaldi (2018). "Parameterizing multi-vent activity at Stromboli Volcano (Aeolian Islands, Italy)". *Bulletin of Volcanology* 80(7). DOI: 10.1007/s00445-018-1239-8.

Sato, H. (1993). "Energy Transportation In One- and Two-Dimensional Scattering Media: Analytic Solutions of the Multiple Isotropic Scattering Model: Energy transportation in one- and two-dimensional scattering media". *Geophysical Journal International* 112(1), pages 141–146. DOI: 10.1111/j.1365-246X.1993.tb01443.x.

Schaefer, L. N., F. Di Traglia, E. Chaussard, Z. Lu, T. Nolesini, and N. Casagli (2019). "Monitoring volcano slope instability with Synthetic Aperture Radar: A review and new data from Pacaya (Guatemala) and Stromboli (Italy) volcanoes".

Earth-Science Reviews 192(March), pages 236–257. DOI: 10.1016/j.earscirev.2019.03.009.

Sens-Schönfelder, C. and U. Wegler (2006). "Passive image interferemetry and seasonal variations of seismic velocities at Merapi Volcano, Indonesia". *Geophysical Research Letters* 33(21), pages 1–5. DOI: 10.1029/2006GL027797.

Silver, P. G., T. M. Daley, F. Niu, and E. L. Majer (2007). "Active source monitoring of cross-well seismic travel time for stress-induced changes". *Bulletin of the Seismological Society of America* 97(1 B), pages 281–293. DOI: 10.1785/0120060120.

Snieder, R. (2006). "The theory of coda wave interferometry". *Pure and Applied Geophysics* 163(2-3), pages 455–473. DOI: 10.1007/s00024-005-0026-6.

Suckale, J., T. Keller, K. V. Cashman, and P. O. Persson (2016). "Flow-to-fracture transition in a volcanic mush plug may govern normal eruptions at Stromboli". *Geophysical Research Letters* 43(23), pages 12, 071–12, 081. DOI: 10.1002/2016GL071501.

Takano, T., T. Nishimura, H. Nakahara, Y. Ohta, and S. Tanaka (2014). "Seismic velocity changes caused by the Earth tide: Ambient noise correlation analyses of small-array data". *Geophysical Research Letters* 41(17), pages 6131–6136. DOI: 10.1002/2014GL060690.

Talwani, P., L. Chen, and K. Gahalaut (2007). "Seismogenic permeability, ks". *Journal of Geophysical Research: Solid Earth* 112(7), pages 1–18. DOI: 10.1029/2006JB004665.

Tibaldi, A., C. Corazzato, T. Apuani, and A. Cancelli (2003). "Deformation at Stromboli volcano (Italy) revealed by rock mechanics and structural geology". *Tectonophysics* 361(3-4), pages 187–204. DOI: 10.1016/S0040-1951(02)00589-9.

Viccaro, M., A. Cannata, F. Cannavò, R. De Rosa, M. Giuffrida, E. Nicotra, M. Petrelli, and G. Sacco (2021). "Shallow conduit dynamics fuel the unexpected paroxysms of Stromboli volcano during the summer 2019". *Scientific Reports* 11(1), pages 1–15. DOI: 10.1038/s41598-020-79558-7.

Voloschina, M., N. Métrich, A. Bertagnini, P. Marianelli, A. Aiuppa, M. Ripepe, and M. Pistolesi (2023). "Explosive eruptions at Stromboli volcano (Italy): a comprehensive geochemical view on magma sources and intensity range". *Bulletin of Volcanology* 85(6), pages 1–21. DOI: 10.1007/s00445-023-01647-y.

Wang, Q. Y., F. Brenguier, M. Campillo, A. Lecointre, T. Takeda, and Y. Aoki (2017). "Seasonal Crustal Seismic Velocity Changes Throughout Japan". *Journal of Geophysical Research: Solid Earth* 122(10), pages 7987–8002. DOI: 10.1002/2017JB014307.

Yamamura, K., O. Sano, H. Utada, Y. Takei, S. Nakao, and Y. Fukao (2003). "Long-term observation of in situ seismic velocity and attenuation". *Journal of Geophysical Research: Solid Earth* 108(B6). DOI: 10.1029/2002jb002005.

Yates, A. S., M. K. Savage, A. D. Jolly, C. Caudron, and I. J. Hamling (2019). "Volcanic, Coseismic, and Seasonal Changes Detected at White Island (Whakaari) Volcano, New Zealand, Using Seismic Ambient Noise". *Geophysical Research Letters* 46(1), pages 99–108. DOI: 10.1029/2018GL080580.

Yates, A. (2023). "Towards accurate monitoring of explosive volcanoes using seismic noiseinterferometry. Volcanology." *Université Savoie Mont Blanc*.

Yi, S., Q. Wang, and W. Sun (2016). "Journal of Geophysical Research : Solid Earth". *Journal of Geophysical Research: Solid Earth*, pages 3782–3803. DOI: 10.1002/2015JB012608.Received.

Zhan, Z., V. C. Tsai, and R. W. Clayton (2013). "Spurious velocity changes caused by temporal variations in ambient noise frequency content". *Geophysical Journal International* 194(3), pages 1574–1581. DOI: 10.1093/gji/ggt170.